SI

Diana Dahliah,† Guillaume Brunin,† Janine George,† Viet-Anh Ha,‡ Gian-Marco Rignanese,† and Geoffroy Hautier*,†

†*Institute of Condensed Matter and Nanoscience, Université catholique de Louvain, Chemin étoiles 8, bte L7.03.01, Louvain-la-Neuve 1348, Belgium*

‡*Institute of Condensed Matter and Nanoscience (IMCN), Université Catholique de Louvain (UCL), Chemin étoiles 8, bte L7.03.01, Louvain-la-Neuve 1348, Belgium*

E-mail: geoffroy.hautier@dartmouth.edu

Table 1 shows the lifetime estimated using the first principle point defect computation and the SRH model for selected PV absorbers that have been examined extensively experimentally and from first principle computations. We analyzed the HSE point defect formation energies data for all possible growth conditions that are provided in literature, assuming all materials at all growth conditions are a p-type absorbers with conduction charge concentration 10^{16} cm^{-3}.

The point defects in PV absorbers that have been intensively studied both in the experiment and in first principle computations and the selected Cu-based PV materials were examined with the PBE exchange-correlation functional.[23,24] The Brillouin zone was sampled using a $2 \times 2 \times 2$ k-point mesh. All intrinsic defects (the cation vacancies, the anion vacancies and the antisites) were considered. Their formation energies were computed at several chemical limits determined by the facets of the DFT phase diagram.[25] In order to overcome the effect on the defect formation energies of the underestimation of the band gap within PBE, the latter was extended to the HSE value. This was achieved by moving both

Table 1: The dominant deep defects and their transition states with respect to VBM, the theoretical life time computed with SRH model, and the experimental conversion efficiency for a set of tested structures with full HSE approach.

material	defect	transition state	theoretical life time(s)	theoretical efficiency(%)	experimental efficiency(%)
Si[1]	Vac Si	(2/0):0.02 (0/-2): 0.91	>> 1	33.3	25.6[2]
CdTe[3]	V_{Cd} , Te_{Cd}	(-2/0):0.36 (0,2):0.42	2.9×10^{-10} – 0.19	21.3−29	22.1[4]
GaAs[5]	As_{Ga} Ga_{As}	(2,1):0.63 (0,-1):0.4	3.9×10^{-11} – 3.2×10^{-4}	9.7-33.3	28.8[2]
Cu_2ZnSnS_4[6]	Sn_{Zn}	(2,1):0.6	1.84×10^{-10}- 3.3×10^{-7}	10.2-20.9	12.6[2]
$CuInSe_2$[7]	Cu_{In}	(0,-1):0.37	2.07×10^{-6}	22.7	23.35[8]
$CuGeSe_2$[7]	Cu_{Ga}	(0,-1):0.33	$6.67\times 10^{-}6$	25.3	23.35[8]
MPI_3[9]	I_i	(-1,1)0.75	2.31×10^{-7}-0.002	24.6-27.7	25.5[10]
InP	Vac_{In}	(0,-1): 0.696769	>> 1	33.3	22.1[2]
Sb_2S_3[11]	Sb_S S_{Sb}	(3,2):0.5 (0,-1):0.67	9.2×10^{-12}-1.2×10^{-8}	8.2 -14.1	6.9[12]
Sb_2Se_3[13]	Vac_{Se} Se_{Sb}	(1,0):0.85) Se_{Sb} (-1,1):0.62	10^{-16}–1.9×10^{-10}	0-6.9	9.2[14]
Cu_2O[15]	V_{Cu}	(0,-1):0.42	3.2×10^{-7}-3.2×10^{-6}	11.7-13.2	9.54[16]
$CuSbS_2$[17]	Cu_{Sb} Sb_{Cu}	(0,-1):0.25 (0,2):1.15	6.64×10^{-10} 7.4×10^{-7}	11.5-19.5	3.22[18]
$ZnSnP_2$[19]	V_P	(0,1): 0.7 (0,-1):1	1.2×10^{-7}–2.8×10^{-6}	19.1–21.7	3.44[20]
SnS[21]	V_S	(0,2) 0.64	1.98×10^{-12}–6.63×10^{-10}	0-8.6	4.36[22]

band edges with respect to a common reference in GGA and HSE computations (more details are given in Refs.[26,27] The plots of the point defect formation energies of PV absorbers that have been intensively studied previously are shown below:

Table 2: The dominant deep defects and their transition states with respect to VBM and the theoretical life time computed with SRH model for the set of tested structures with GGA+HSE approach.

material	defect	transition state	theoretical life time(s)	experimental efficiency(%)
Si	–	–	$\gg 1$	25.6[2]
CdTe	V_{Cd}	(-2, -1): 0.58	2.34×10^{-3} – $\gg$1	22.1[?]
InP	–	–	$\gg 1$	22.1[2]
GaP	Ga_P, P_{Ga}	(0,1):0.76, (1,2):0.717	4.8×10^{-11}– 2×10^{-4}	2.42[28]
ZnTe	V_{Zn}	(0,-1):0.48	5.53×10^{-8}–4.4×10^{-6}	5.9[29]
$CuSbS_2$	Sb_{Cu}	(1,2):0.90594	7.72×10^{-9}–3.07×10^{-7}	3.22[18]
Sb_2S_3	v_S	(1,2):0.87	1.56×10^{-18}–1.87×10^{-12}	6.9[12]
Sb_2Se_3	V_{Se}	(0,2):0.65	2.48×10^{-11}–4.11×10^{-9}	9.2[14]
SbSI	V_S, V_I Sb_S	(0,2):0.94,(-1,1):1.29, (1,3): 0.87	2.48×10^{-26}– 1.21×10^{-20}	3.5[30]
SnS	V_S	(1,2):0.543 8.2×10^{-13}–3.4×10^{-10}		4.36[22]
SnSe	Se_{Sn}	(2,3): 0.731	2.18×10^{-18}–1.46×10^{-10}	6.44[31]
$ZnSnP_2$	V_P	(0,1):0.3	1.08×10^{-8}– 6.72×10^{-7}	3.44[20]
Bi2S3	V_S	(0,1):1.1	3.54×10^{-18}– 3.4×10^{-14}	5.9[32]
Cu_2O	–	–	$\gg 1$	9.54[16]

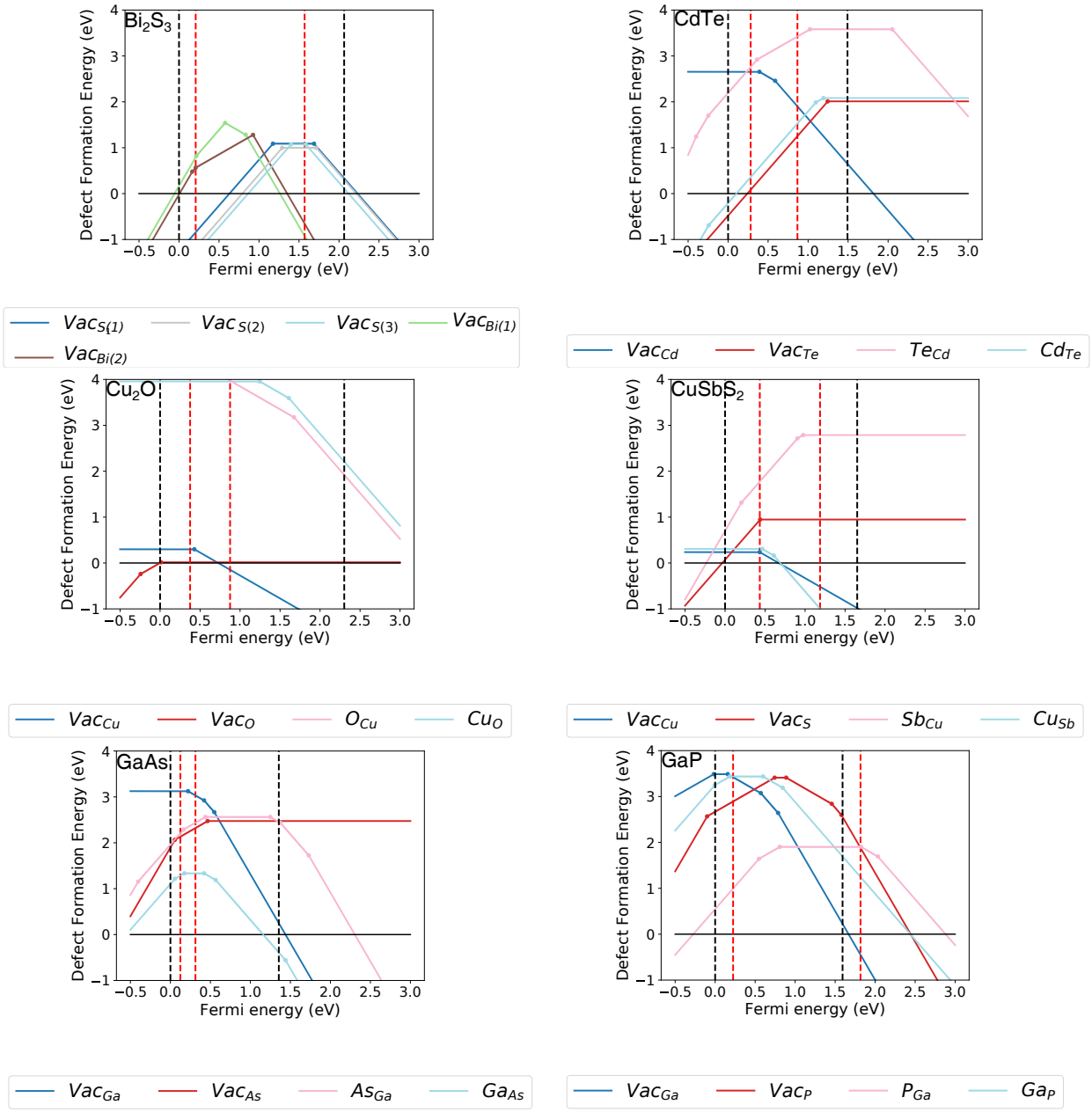

Figure 1: GGA+HSE intrinsic defect formation energies as a function of the Fermi energy for Bi_2S_3, CdTe, Cu_2O, $CuSbS_2$, GaAs, and GaP. The zero in Fermi energy corresponds to the VBM, and the CBM is indicated with a vertical dashed line.

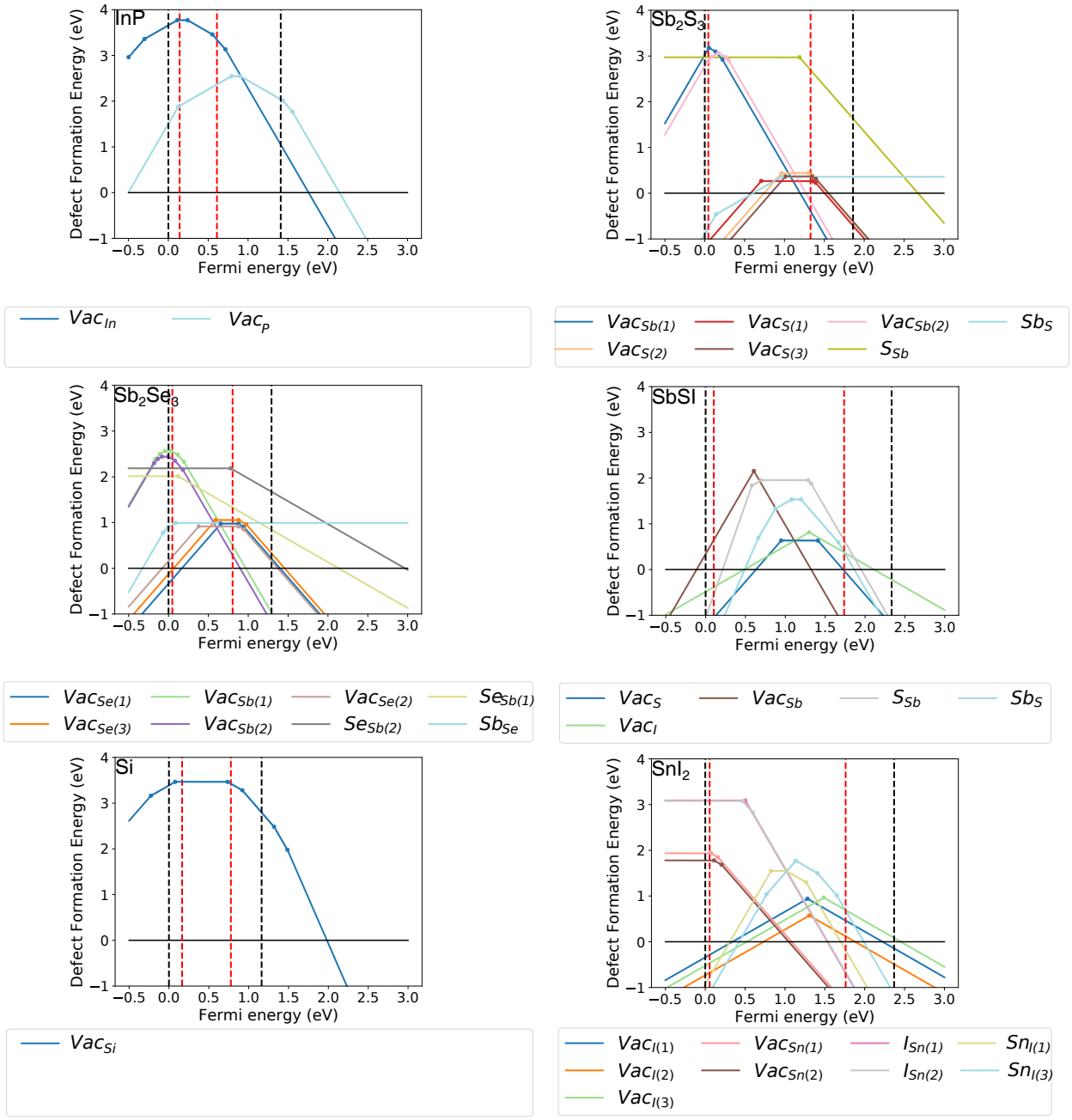

Figure 2: GGA+HSE intrinsic defect formation energies as a function of the Fermi energy for InP, Sb_2S_3, Sb_2Se_3, SbSi, Si, SnI_2. The zero in Fermi energy corresponds to the VBM, and the CBM is indicated with a vertical dashed line.

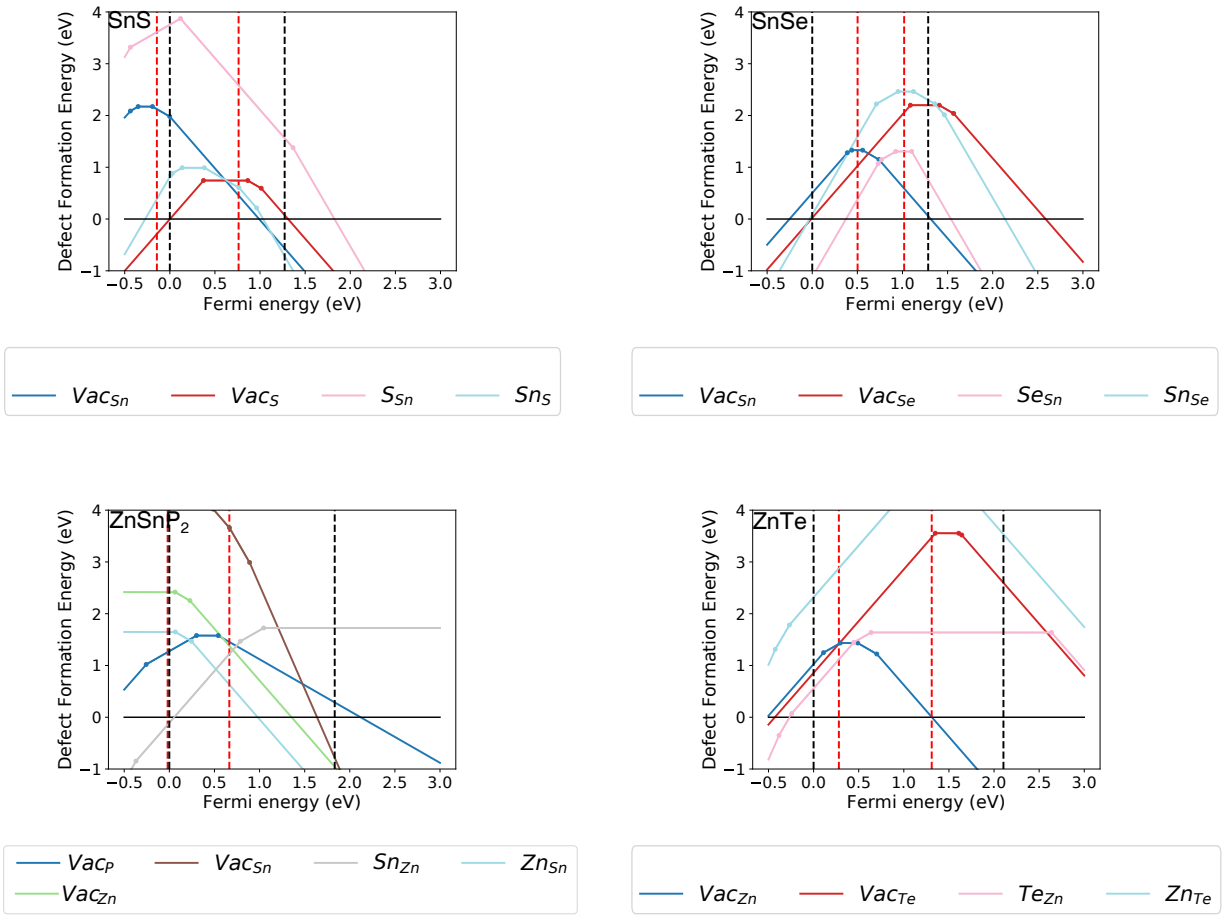

Figure 3: GGA+HSE intrinsic defect formation energies as a function of the Fermi energy for SnS, SnSe, $ZnSnP_2$, ZnTe. The zero in Fermi energy corresponds to the VBM, and the CBM is indicated with a vertical dashed line.

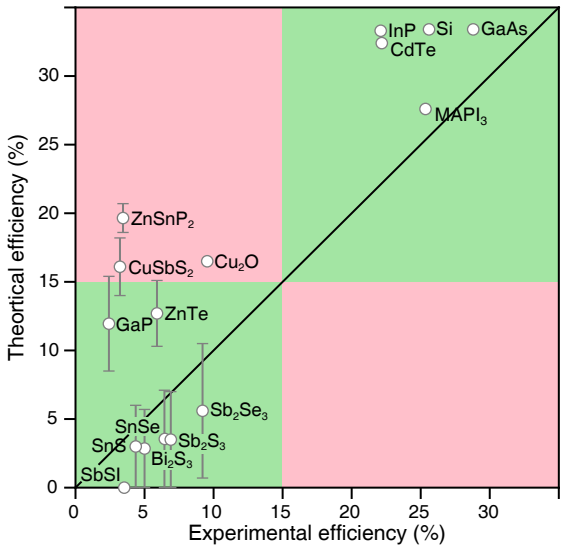

Figure 4: Theoretical efficiency from GGA+HSE approach for selected materials compared to their experimental efficiency. The range in theoretical efficiency corresponds to different growing conditions, hence different defects present in each material.The middle of the range is indicated by white circles. The green regions, indicating efficiencies lower (resp. larger) than 15 %, correspond to correctly predicted low- (resp. high-) efficiency materials. The red regions correspond to false positives (upper left) and negatives (lower right).

Table 3: materials Project identification number, Formula, space group (SG), ,stability measured by energy above hull (E_{hull}) in the phase diagram (meV/atom) , three principal hole effective masses m_p1, m_{p2} and m_{3p} (m_o-free electron mass),also the three principal electron effective masses, PBE fundamental (E_g) and direct gaps (E_g^d) and the corrected band gap with hybrid functional (HSE06).

mpID	formula	SG	E_{hull}	m_{p1}	m_{p2}	m_{p3}	m_{n1}	m_{n2}	m_{n3}	E_g	E_g^d	Δgap	HSE-gap
17916	Y3CuGeSe7	P6_3	0	0.659	0.659	3.915	0.28	0.645	0.645	1.118	1.118	0	1.9805
8446	K2CuP	Cmcm	0	2.175	2.744	3.624	0.227	0.754	0.812	1.142	1.223	0.081	1.9847
15684	K2CuAs	Cmcm	0	2.06	2.564	2.801	0.292	0.295	0.309	1.068	1.176	0.109	2.037
14205	K3Cu3As2	R-3m	0	1.272	1.272	1.922	0.36	0.36	0.761	1.296	1.317	0.037	2.0842
7439	K3Cu3P2	R-3m	0	1.236	1.236	2.144	0.392	0.392	0.705	1.309	1.345	0.055	2.1388
8017	AlCuTe2	I-42d	0	0.492	0.763	0.764	0.107	0.119	0.12	1.024	1.019	0	2.2581
3934	Cu3PS4	Pmn2_1	0	0.734	1.304	1.478	0.268	0.448	0.466	1.02	1.033	0.012	2.3069
568954	Nd3CuGeSe7	P6_3	0	0.765	0.765	4.176	0.357	0.804	0.804	1.194	1.205	0.012	2.0877
570226	Sm3CuGeSe7	P6_3	0	0.702	0.702	3.861	0.336	0.741	0.741	1.165	1.17	0.008	2.0465
505558	Dy3CuGeSe7	P6_3	0	0.641	0.641	3.651	0.29	0.636	0.636	1.113	1.115	0.002	2.0434
510011	La3CuGeSe7	P6_3	0	1.135	1.135	4.399	0.381	0.869	0.869	1.185	1.222	0.038	2.2571
571347	Pr3CuGeSe7	P6_3	0	0.796	0.796	4.275	0.376	0.848	0.848	1.206	1.219	0.014	2.1428
567428	Tb3CuGeSe7	P6_3	0	0.659	0.659	3.68	0.293	0.648	0.648	1.127	1.127	0	2.059
7374	Ba(CuO)2	I4_1/amd	0	1.008	3.786	3.796	0.301	0.302	0.815	1.379	1.379	0	2.5552
18685	SrCu2GeS4	P3_221	0	0.836	0.836	4.411	0.191	0.191	0.257	1.05	1.055	0.009	2.5616

12954	CuBS2	I-42d	0	0.932	1.071	1.071	0.399	0.402	0.742	1.743	1.743	0	2.7088
4979	AlCuS2	I-42d	0	1.018	1.759	1.76	0.21	0.233	0.234	1.694	1.694	0	3.0779
555978	Sm3CuGeS7	P6_3	0	0.935	0.935	4.779	0.733	0.892	0.892	1.794	1.864	0.091	2.8971
7639	Na2CuP	Cmcm	0	0.619	0.731	1.545	0.1	0.852	0.898	0.677	0.788	0.13	1.826
15685	Na2CuAs	Cmcm	0	0.57	0.585	1.438	0.159	0.716	0.793	0.678	0.714	0.055	1.707
557225	Cu6GeWS8	P6_3mc	0	1.444	1.787	1.787	0.265	0.265	0.313	0.815	0.815	0	1.93
27999	K5CuSb2	R-3m	0	2.319	3.378	3.378	0.19	0.219	0.219	0.751	0.882	0.135	1.6232
8016	AlCuSe2	I-42d	0	0.494	1.037	1.037	0.121	0.133	0.136	0.896	0.892	0	2.2932
5238	GaCuS2	I-42d	0	0.533	0.951	0.952	0.137	0.151	0.152	0.704	0.706	0	2.25
6449	CdSi(CuS2)2	Pmn2_1	0	0.534	2.18	2.771	0.186	0.19	0.249	0.98	0.98	0	2.4026
17947	CuBiPbS3	P3_121	0	0.951	0.951	3.3843	0.193	0.193	0.245	0.971	0.974	0.008	2.4315
22914	CuCl	F-43m	0	1.784	1.784	1.784	0.252	0.252	0.252	0.561	0.561	0	2.4162
569168	Ba6NaCu3Te14	P6_3/mcm	0	0.688	2.057	2.057	0.207	0.538	0.538	0.617	0.634	0.032	1.236
17063	BaLaCuTe3	Pnma	0	0.477	1.103	1.352	0.352	0.704	0.879	0.82	0.82	0	1.2931
654109	BaCu4S3	Pnma	0	0.187	1.139	2.234	0.138	0.227	0.382	0.452	0.452	0	1.5248
12364	BaCu2SnSe4	Ama2	0	0.705	2.946	3.416	0.116	0.183	0.235	0.424	0.45	0.026	1.6018
13982	CdCu2GeS4	Pmn2_1	0	0.541	1.98	2.16	0.122	0.127	0.133	0.362	0.362	0	1.6776
23287	CuCl	Pa3	0	3.188	3.188	3.188	0.248	0.248	0.248	0.444	0.444	0	3.306
7436	KCuTe	P6_3/mmc	0	0.338	0.338	6.601	0.093	0.093	0.432	0.604	0.604	0	1.5257

29396	Cu2PbO2	C2/c	0	1.081	3.287	6.072	0.351	0.461	0.561	0.646	0.773	0.144	
29136	Sr6Cu3N5	P4_2mc	0	1.525	5.859	5.859	0.422	0.607	0.607	0.483	0.608	0.132	1.6424
9194	SmCuSeO	P4/nmm	1.18	0.653	0.653	2.936	0.224	0.224	0.339	1.286	1.286	0	2.6161
22863	CuI	P4/nmm	1.63	0.73	0.73	1.634	0.231	0.231	0.244	1.572	1.572	0	2.9193
570081	CuI	P-3m1	1.63	2	2	4.858	0.206	0.277	0.277	1.634	1.634	0	2.9916
32750	CuI	R3m	1.63	1.09	1.09	1.393	0.163	0.173	0.173	1.164	1.164	0	2.758
673245	CuI	Pc	1.63	0.895	0.916	1.054	0.164	0.173	0.176	1.145	1.145	0	2.7244
569346	CuI	P6_3mc	1.63	1.053	1.053	1.513	0.159	0.179	0.179	1.217	1.217	0	2.7432
22895	CuI	F-43m	1.63	0.863	0.863	0.863	0.174	0.174	0.174	1.136	1.136	0	2.6699
5970	Ba(CuS)2	Pnma	2.40	0.347	1.73	2.168	0.207	0.256	0.695	0.903	0.903	0	1.9518
542302	CuBi3PbS6	Pmc2_1	4.05	1.118	1.876	2.196	0.212	0.55	0.627	0.622	0.622	0	1.4473
16179	SrCu2GeSe4	Ama2	4.22	0.425	3.078	3.774	0.208	0.284	0.435	0.592	0.723	0.135	1.8776
23431	CsCu2I3	Cmcm	4.27	1.236	2.206	2.361	0.268	0.283	0.313	1.901	1.901	0	3.364
21390	La2InCuSe5	Pnma	7.301	1.15	2.24	4.664	0.247	0.251	0.882	0.509	0.509	0	1.4084
23353	Cu2HgI4	I-42m	7.56	1.059	1.059	1.842	0.225	0.226	0.252	0.565	0.559	0	1.8524
624191	CuBiPbS3	Pnma	9.30	0.766	0.942	1.097	0.276	0.323	0.431	0.633	0.651	0.038	1.735
7434	NaCuTe	P4/nmm	9.62	0.425	0.425	1.526	0.113	0.113	0.113	0.633	0.633	0	1.6734
15895	SiCu2S3	Cc	10.07	0.609	1.678	2.926	0.187	0.3	0.302	1.112	1.112	0	1.7747
18126	Tb3CuSnSe7	P6_3	12.61	0.647	0.647	4.058	0.253	0.862	0.862	1.018	1.015	0	1.866

9304	DyCuSeO	P4/nmm	15.42	0.599	0.599	2.615	0.197	0.197	0.324	1.18	1.18	0	2.5154
510539	Dy3CuSnSe7	P6_3	17.91	0.671	0.671	4.236	0.232	0.809	0.809	0.993	0.99	0	1.8972
37405	Al5CuSe8	F-43m	18.78	0.804	0.804	0.804	0.129	0.129	0.129	0.518	0.612	0.098	1.6203
774712	LiCuS	P6_3/mmc	19.71	0.365	0.365	4.864	0.145	0.145	0.606	0.851	0.851	0	2.103
675180	ErCuSe2	P3m1	20.28	0.586	0.586	0.927	0.193	0.193	0.728	1.05	1.05	0	2.3208
542426	CuHgSI	Pna2_1	20.43	0.93	1.815	2.792	0.174	0.192	0.213	0.445	0.445	0	Hg is toxic
754501	Ca(CuO)2	I4_1/amd	32.65	1.255	1.261	4.401	0.208	0.209	0.392	1.525	1.525	0	2.753
4473	Ba(CuSe)2	Pnma	34.40	0.224	1.456	1.733	0.122	0.137	0.279	0.486	0.486	0	1.6063
22917	CuBr	P4/nmm	41.42	1.642	1.642	3.283	0.269	0.269	0.306	0.995	0.995	0	2.5011
32880	CuBr	I-4m2	41.42	1.437	1.438	1.449	0.163	0.166	0.167	0.448	0.448	0	2.987
22913	CuBr	F-43m	41.42	1.33	1.33	1.33	0.17	0.17	0.17	0.486	0.486	0	2.987
5546	BaCu2GeS4	Pmn2_1	42.85	1.595	2.004	3.245	0.179	0.203	0.204	0.598	0.598	0	2.4315
5546	Cu8GeS6	Pnm2_1	43	1.595	2.004	3.245	0.179	0.203	0.204	0.598	0.598	0	1.8792
753826	LiCuS	Pnma	49.41	0.419	1.208	1.312	0.244	0.246	0.298	1.076	1.076	0	2.4835
766467	LiCuS	Pbcn	49.41	2.215	2.931	2.975	0.315	0.321	0.325	1.291	1.291	0	2.5327
774736	LiCuS	Cc	49.41	1.682	2.939	3.753	0.244	0.28	0.474	1.58	1.582	0.017	2.6477
10428	Si(Cu4Se3)2	Pmn2_1	52.24	1.386	1.858	2.572	0.126	0.13	0.162	0.409	0.421	0.012	1.4943
753737	Li3CuS2	Pbcn	69.33	0.532	0.537	2.219	0.267	0.27	0.352	1.981	1.981	0	3.5525
766447	Li2Cu4S3	Pnma	70.87	0.263	0.975	2.617	0.187	0.283	0.438	0.753	0.753	0	2.0263

6166	PrCuSO	P4/nmm	94.6	0.977	0.977	4.89	0.324	0.324	0.479	1.642	1.642	0	3.0414
542314	NdCuSO	P4/nmm	98.12	0.945	0.945	4.35	0.318	0.318	0.47	1.614	1.614	0	3.0661

composition	Al_2CuSe_3
MP-id	37405
space group	$F\bar{4}3m$
hole effective mass	[0.804, 0.804, 0.804]
electron effective mass	[0.129, 0.129, 0.129]
HSE band gap (indirect/direct) (eV)	1.651/ 1.66
energy above hull (eV/atom)	0.02
life time (ns)	$[1.08\times 10^{-2} - 3.67\times 10^{+2}]$

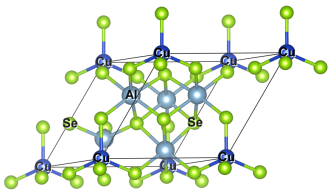

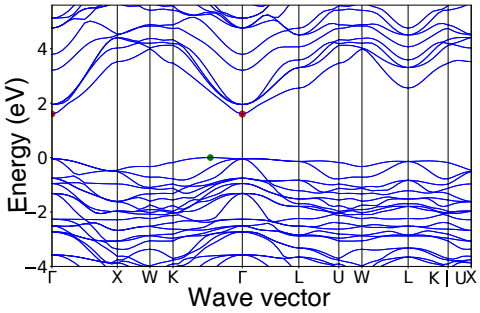

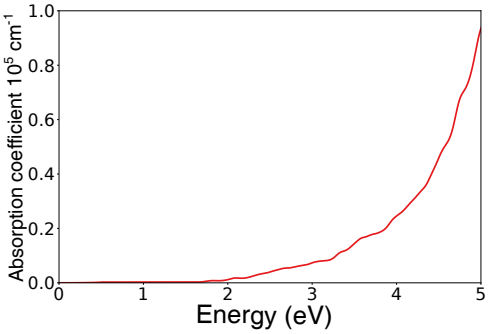

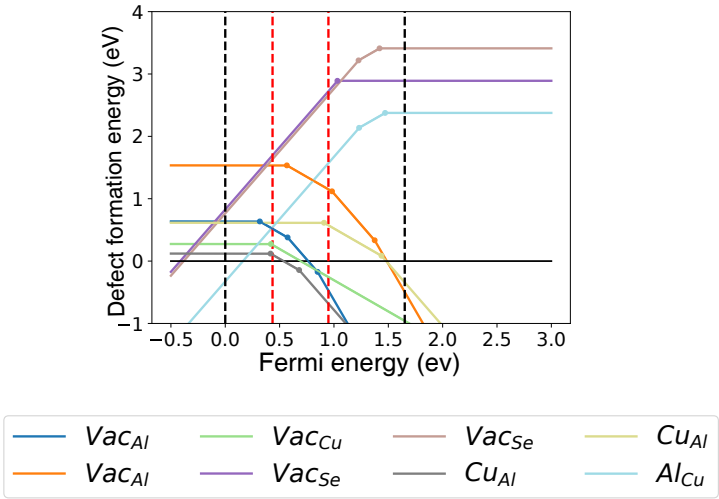

References

(1) Śpiewak, P.; Kurzydłowski, K. J. Formation and migration energies of the vacancy in Si calculated using the HSE06 range-separated hybrid functional. *Physical Review B* **2013**, *88*, 195204.

(2) Polman, A.; Knight, M.; Garnett, E. C.; Ehrler, B.; Sinke, W. C. Photovoltaic materials: Present efficiencies and future challenges. *Science* **2016**, *352*, aad4424.

(3) Yang, J.-H.; Park, J.-S.; Kang, J.; Metzger, W.; Barnes, T.; Wei, S.-H. Tuning the Fermi level beyond the equilibrium doping limit through quenching: The case of CdTe. *Physical Review B* **2014**, *90*, 245202.

composition	$AlCuTe_2$
MP-id	8017
space group	$I\bar{4}2d$
hole effective mass	[0.492, 0.763, 0.764]
electron effective mass	[0.107, 0.119, 0.12]
HSE band gap (indirect/direct) (eV)	2.143/ 2.143
energy above hull (eV/atom)	0.00
life time (ns)	$[1.8\times 10^{-4} - 6.5\times 10^{-4}]$

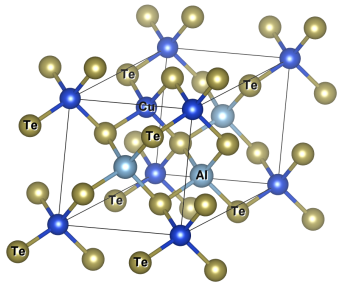

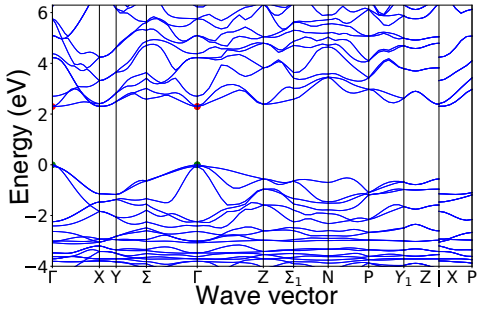

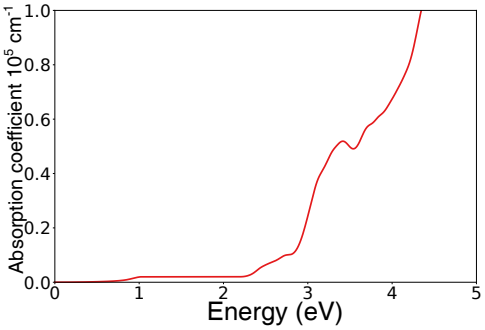

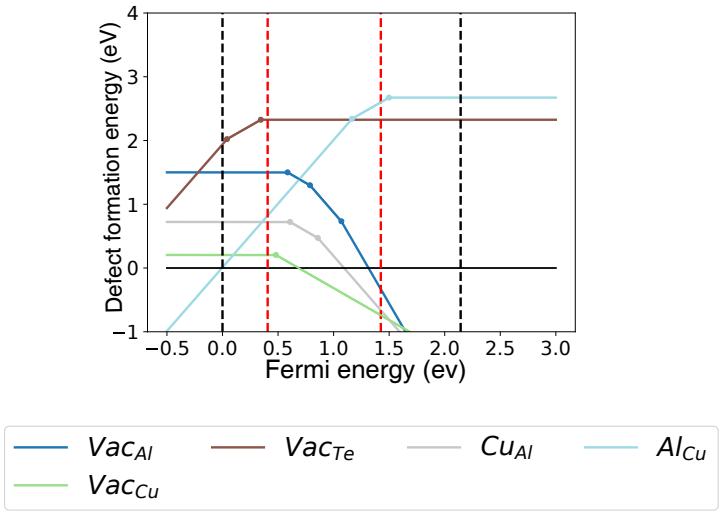

(4) Romeo, A.; Artegiani, E. CdTe-Based Thin Film Solar Cells: Past, Present and Future. *Energies* **2021**, *14*, 1684.

(5) Komsa, H.-P.; Pasquarello, A. Intrinsic defects in GaAs and InGaAs through hybrid functional calculations. *Physica B: Condensed Matter* **2012**, *407*, 2833–2837.

(6) Kim, S.; Park, J.-S.; Hood, S. N.; Walsh, A. Lone-pair effect on carrier capture in Cu 2 ZnSnS 4 solar cells. *Journal of Materials Chemistry A* **2019**, *7*, 2686–2693.

(7) Huang, B.; Chen, S.; Deng, H.-X.; Wang, L.-W.; Contreras, M. A.; Noufi, R.; Wei, S.-H. Origin of Reduced Efficiency in Cu (In, Ga) Se _2 Solar Cells With High Ga Concentration: Alloy Solubility Versus Intrinsic Defects. *IEEE Journal of Photovoltaics* **2013**, *4*, 477–482.

(8) Nakamura, M.; Yamaguchi, K.; Kimoto, Y.; Yasaki, Y.; Kato, T.; Sugimoto, H. Cd-free

composition	$BaCu_2S_2$
MP-id	5970
space group	Pnma
hole effective mass	[0.347, 1.73, 2.168]
electron effective mass	[0.207, 0.256, 0.695]
HSE band gap (indirect/direct) (eV)	2.061/2.069
energy above hull (eV/atom)	0.002
life time (ns)	>>1

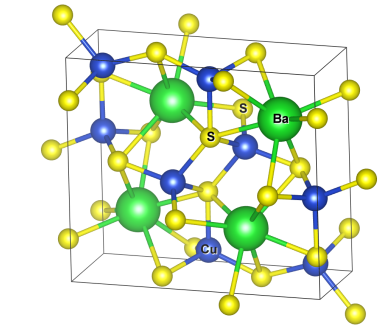

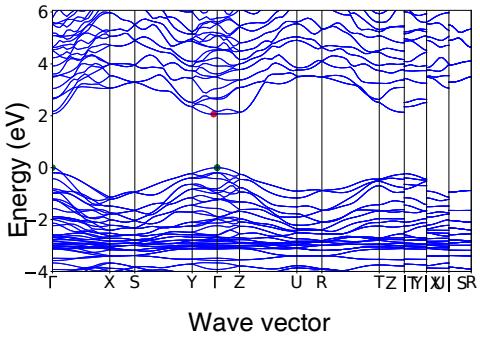

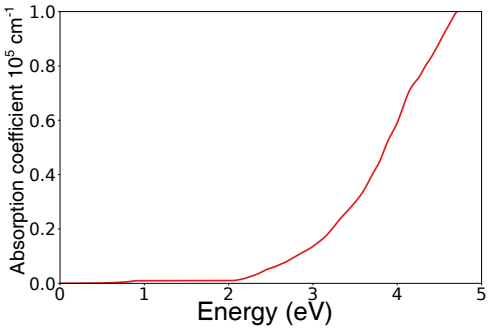

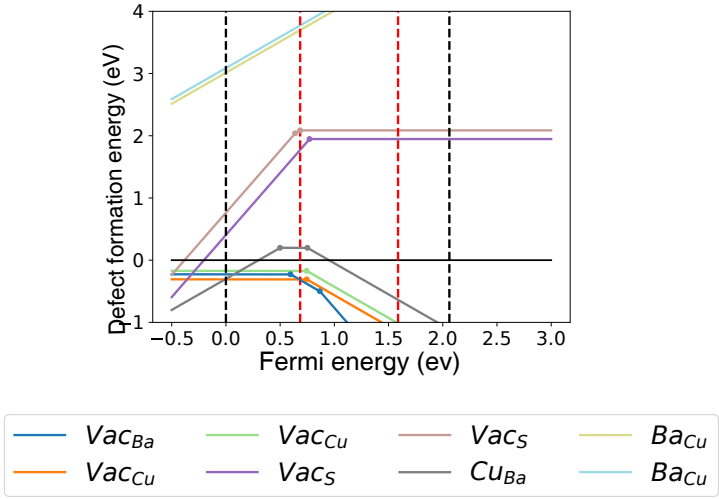

Cu (In, Ga)(Se, S) 2 thin-film solar cell with record efficiency of 23.35%. *IEEE Journal of Photovoltaics* **2019**, *9*, 1863–1867.

(9) Meggiolaro, D.; De Angelis, F. First-principles modeling of defects in lead halide perovskites: best practices and open issues. *ACS Energy Letters* **2018**, *3*, 2206–2222.

(10) Energy, N. T. Best research-cell efficiency chart. 2020; `https://www.nrel.gov/pv/cell-efficiency.html`.

(11) Guo, L.; Zhang, B.; Li, S.; Zhang, Q.; Buettner, M.; Li, L.; Qian, X.; Yan, F. Scalable and efficient Sb2S3 thin-film solar cells fabricated by close space sublimation. *APL Materials* **2019**, *7*, 041105.

(12) Han, J.; Wang, S.; Yang, J.; Guo, S.; Cao, Q.; Tang, H.; Pu, X.; Gao, B.; Li, X. Solution-Processed Sb2S3 Planar Thin Film Solar Cells with a Conversion Efficiency of

composition	$BaCu_2Se_2$
MP-id	4473
space group	Pnma
hole effective mass	[0.224, 1.456, 1.733]
electron effective mass	[0.122, 0.137, 0.279]
HSE band gap (indirect/direct) (eV)	1.627 / 1.627
energy above hull (eV/atom)	0.034
life time (ns)	>>1

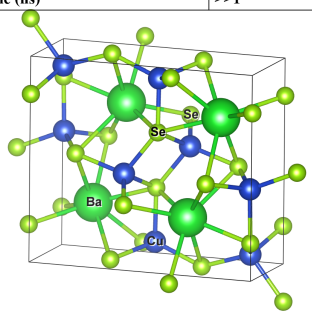

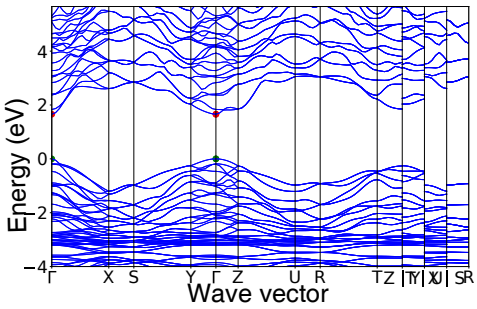

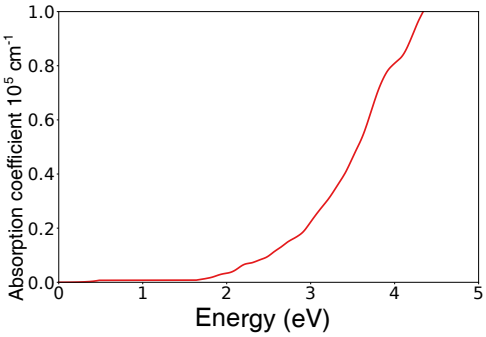

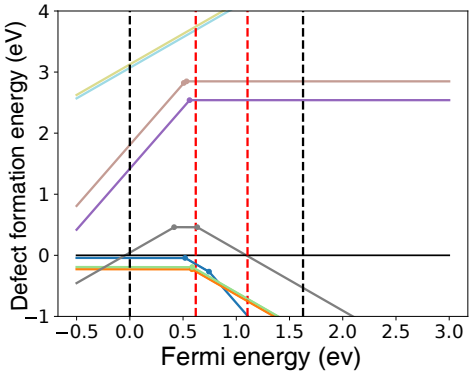

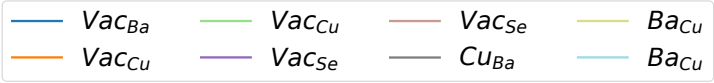

6.9% at an Open Circuit Voltage of 0.7 V Achieved via Surface Passivation by a SbCl3 Interface Layer. *ACS Applied Materials & Interfaces* **2019**, *12*, 4970–4979.

(13) Savory, C. N.; Scanlon, D. O. The complex defect chemistry of antimony selenide. *Journal of Materials Chemistry A* **2019**, *7*, 10739–10744.

(14) Li, Z.; Liang, X.; Li, G.; Liu, H.; Zhang, H.; Guo, J.; Chen, J.; Shen, K.; San, X.; Yu, W.; Schropp, R. E.; Mai, Y. 9.2%-efficient core-shell structured antimony selenide nanorod array solar cells. *Nature Communications* **2019**, *10*, 1–9.

(15) Scanlon, D. O.; Morgan, B. J.; Watson, G. W.; Walsh, A. Acceptor levels in p-type Cu 2 O: rationalizing theory and experiment. *Physical Review Letters* **2009**, *103*, 096405.

(16) Liu, Y.; Zhu, J.; Cai, L.; Yao, Z.; Duan, C.; Zhao, Z.; Zhao, C.; Mai, W. Solution-Processed High-Quality Cu2O Thin Films as Hole Transport Layers for Pushing the

composition	$BaCu_2SnSe_4$
MP-id	12364
space group	Ama2
hole effective mass	[0.705, 2.946, 3.416]
electron effective mass	[0.116, 0.183, 0.235]
HSE band gap (indirect/direct) (eV)	1.577/1.577
energy above hull (eV/atom)	0.00
life time (ns)	>>1

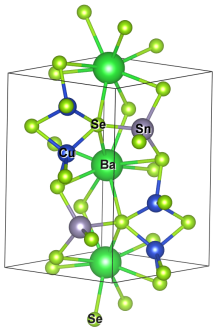

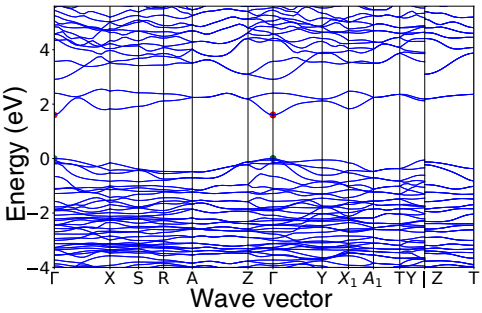

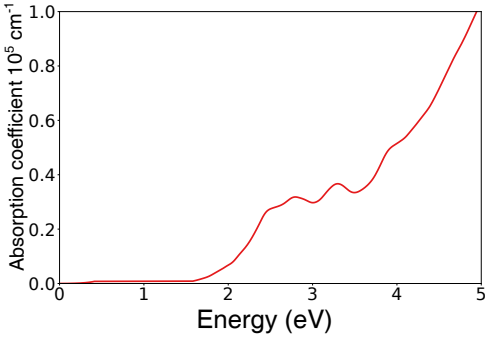

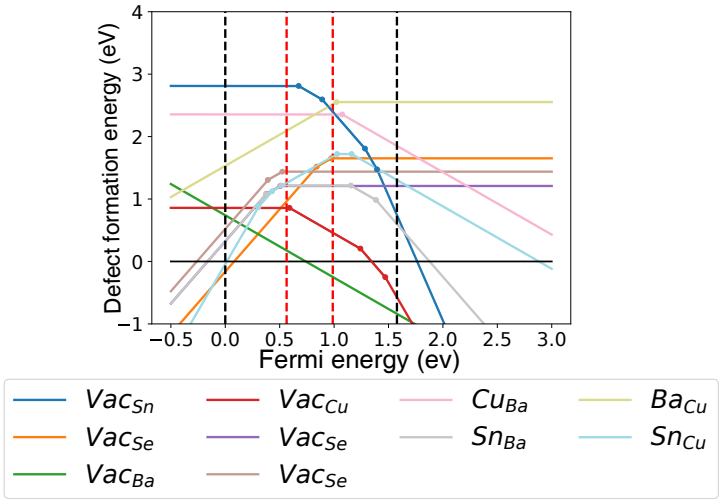

Conversion Efficiency Limit of Cu2O/Si Heterojunction Solar Cells. *Solar RRL* **2020**, *4*, 1900339.

(17) Yang, B.; Wang, L.; Han, J.; Zhou, Y.; Song, H.; Chen, S.; Zhong, J.; Lv, L.; Niu, D.; Tang, J. CuSbS2 as a promising earth-abundant photovoltaic absorber material: a combined theoretical and experimental study. *Chemistry of Materials* **2014**, *26*, 3135–3143.

(18) Banu, S.; Ahn, S. J.; Ahn, S. K.; Yoon, K.; Cho, A. Fabrication and characterization of cost-efficient CuSbS2 thin film solar cells using hybrid inks. *Solar Energy Materials and Solar Cells* **2016**, *151*, 14–23.

(19) Kumagai, Y.; Choi, M.; Nose, Y.; Oba, F. First-principles study of point defects in chalcopyrite ZnSnP2. *Physical Review B* **2014**, *90*, 125202.

composition	$BaCu_4S_3$
MP-id	654109
space group	Pnma
hole effective mass	[0.187, 1.139, 2.234]
electron effective mass	[0.138, 0.227, 0.382]
HSE band gap (indirect/direct) (eV)	1.61/ 1.61
energy above hull (eV/atom)	0.00
life time (ns)	--

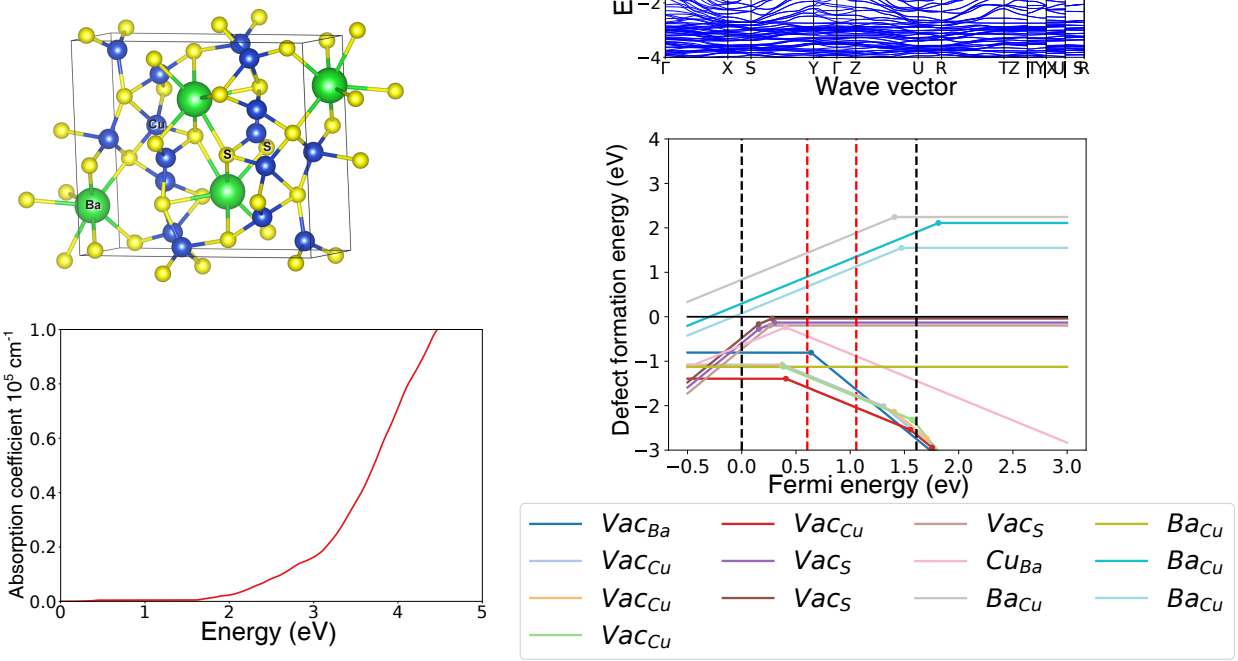

(20) Akari, S.; Chantana, J.; Nakatsuka, S.; Nose, Y.; Minemoto, T. ZnSnP2 solar cell with (Cd, Zn) S buffer layer: Analysis of recombination rates. *Solar Energy Materials and Solar Cells* **2018**, *174*, 412–417.

(21) Polizzotti, A.; Faghaninia, A.; Poindexter, J. R.; Nienhaus, L.; Steinmann, V.; Hoye, R. L.; Felten, A.; Deyine, A.; Mangan, N. M.; Correa-Baena, J. P.; Sik Shin, S.; Jaffer, S.; Bawendi, M. G.; Lo, C.; Buonassisi, T. Improving the carrier lifetime of tin sulfide via prediction and mitigation of harmful point defects. *The journal of physical chemistry letters* **2017**, *8*, 3661–3667.

(22) Baig, F.; Khattak, Y. H.; Soucase, B. M.; Beg, S.; Khani, N. A. K. Efficiency limits of SnS thin film solar cells. *Materials Focus* **2018**, *7*, 807–813.

(23) Perdew, J. P.; Burke, K.; Ernzerhof, M. Generalized gradient approximation made

composition	$CdCu_2GeS_4$
MP-id	13982
space group	$Pnm2_1$
hole effective mass	[0.541, 1.98, 2.16]
electron effective mass	[0.122, 0.127, 0.133]
HSE band gap (indirect/direct) (eV)	1.764/ 1.764
energy above hull (eV/atom)	0.00
life time (ns)	>>1

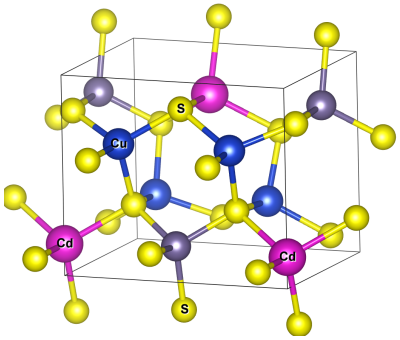

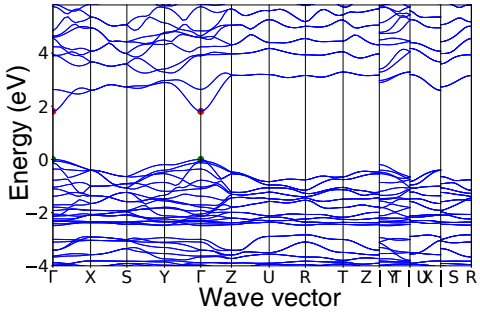

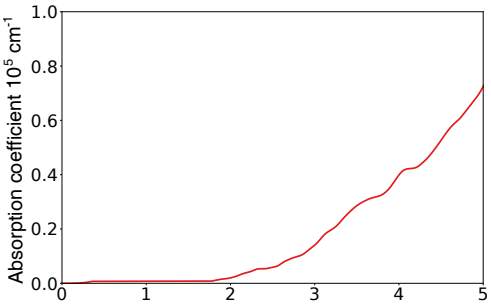

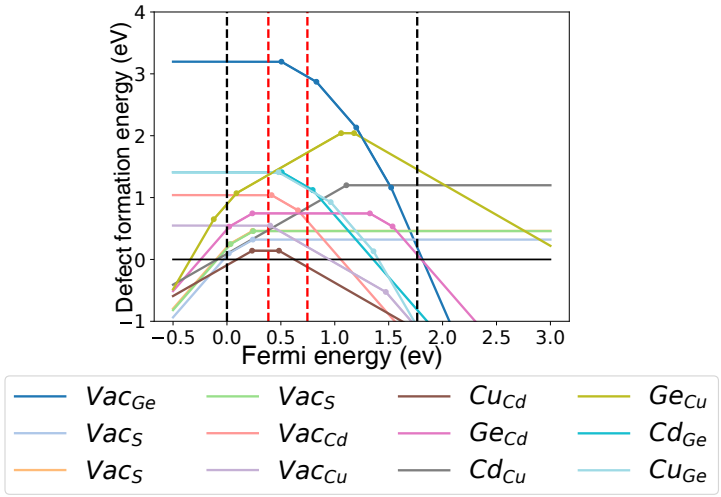

simple. *Physical Review Letters* **1996**, *77*, 3865.

(24) Freysoldt, C.; Grabowski, B.; Hickel, T.; Neugebauer, J.; Kresse, G.; Janotti, A.; Van de Walle, C. G. First-principles calculations for point defects in solids. *Reviews of Modern Physics* **2014**, *86*, 253.

(25) Zhang, S.; Northrup, J. E. Chemical potential dependence of defect formation energies in GaAs: Application to Ga self-diffusion. *Physical Review Letters* **1991**, *67*, 2339.

(26) Alkauskas, A.; Broqvist, P.; Pasquarello, A. Defect energy levels in density functional calculations: Alignment and band gap problem. *Physical Review Letters* **2008**, *101*, 046405.

(27) Alkauskas, A.; Broqvist, P.; Pasquarello, A. Defect levels through hybrid density functionals: Insights and applications. *Physica Status Solidi (b)* **2011**, *248*, 775–789.

composition	$SiCu_2S_3$
MP-id	15895
space group	Cc
hole effective mass	[0.609, 1.678, 2.926]
electron effective mass	[0.187, 0.3, 0.302]
HSE band gap (indirect/direct) (eV)	2.557/ 2.557
energy above hull (eV/atom)	0.009
life time (ns)	5.33×10^{-2}

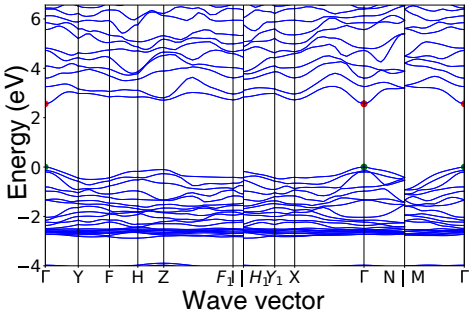

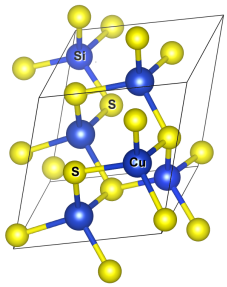

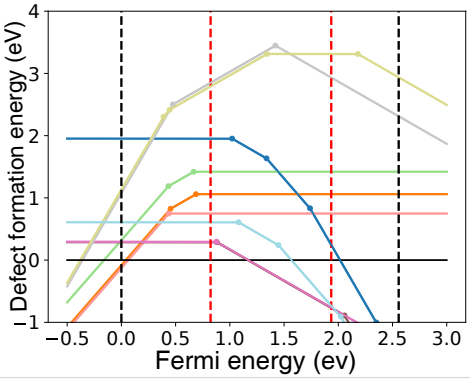

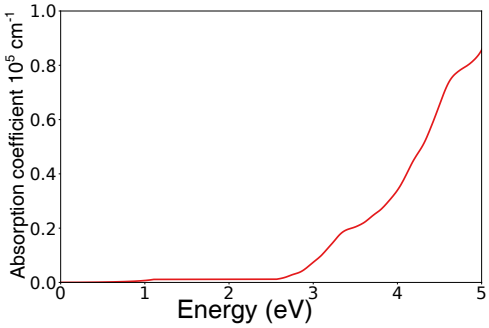

(28) Lu, X.; Huang, S.; Diaz, M. B.; Kotulak, N.; Hao, R.; Opila, R.; Barnett, A. Wide band gap gallium phosphide solar cells. *IEEE Journal of Photovoltaics* **2012**, *2*, 214–220.

(29) Lee, K. S.; Oh, G.; Chu, D.; Pak, S. W.; Kim, E. K. High power conversion efficiency of intermediate band photovoltaic solar cell based on Cr-doped ZnTe. *Solar Energy Materials and Solar Cells* **2017**, *170*, 27–32.

(30) Nie, R.; Yun, H.-s.; Paik, M.-J.; Mehta, A.; Park, B.-w.; Choi, Y. C.; Seok, S. I. Efficient Solar Cells Based on Light-Harvesting Antimony Sulfoiodide. *Advanced Energy Materials* **2018**, *8*, 1701901.

(31) Shi, W.; Gao, M.; Wei, J.; Gao, J.; Fan, C.; Ashalley, E.; Li, H.; Wang, Z. Tin selenide (SnSe): growth, properties, and applications. *Advanced Science* **2018**, *5*, 1700602.

(32) Xu, B.; Wang, G.; Fu, H. 23327Enhanced photoelectric conversion efficiency of dye-

composition	Cu_3PS_4
MP-id	3934
space group	$pnm2_1$
hole effective mass	[0.734, 1.304, 1.478]
electron effective mass	[0.268, 0.448, 0.466]
HSE band gap (indirect/direct) (eV)	2.51 / 2.60
energy above hull (eV/atom)	0.00
life time (ns)	$[1.34\times 10^{-1} - 2.8\times 10^{+2}]$

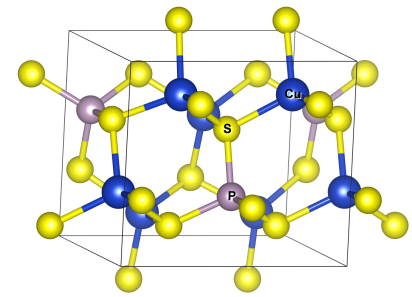

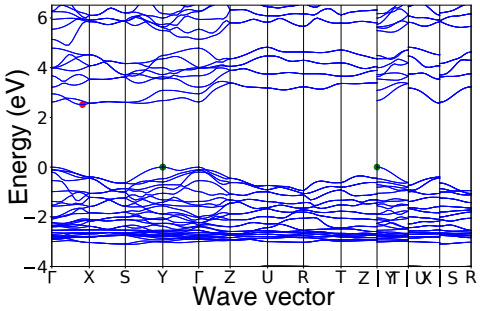

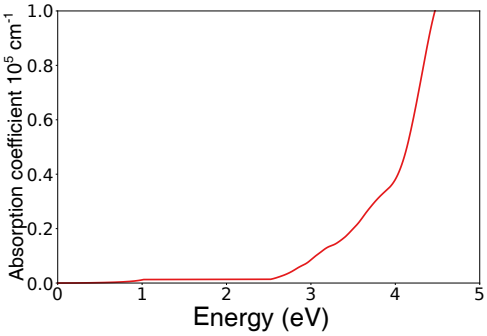

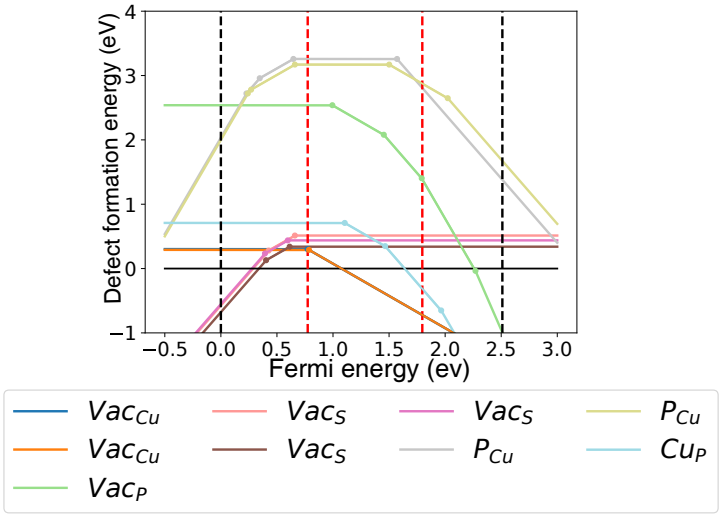

sensitized solar cells by the incorporation of flower-like Bi 2 S 3: Eu 3+ sub-microspheres. *Scientific reports* **2016**, *6*, 1–9.

(33) Brunin, G.; Miranda, H. P. C.; Giantomassi, M.; Royo, M.; Stengel, M.; Verstraete, M. J.; Gonze, X.; Rignanese, G.-M.; Hautier, G. Phonon-limited electron mobility in Si, GaAs, and GaP with exact treatment of dynamical quadrupoles. *Phys. Rev. B* **2020**, *102*, 094308.

composition	**Cu_6GeWS_8**
MP-id	**557225**
space group	**$P6_3mc$**
hole effective mass	**[1.444, 1.787, 1.787]**
electron effective mass	**[0.265, 0.265, 0.313]**
HSE band gap (indirect/direct) (eV)	**2.19/2.19**
energy above hull (eV/atom)	**0.00**
life time (ns)	**$[3.74\times 10^{-5} - 3.6\times 10^{-1}]$**

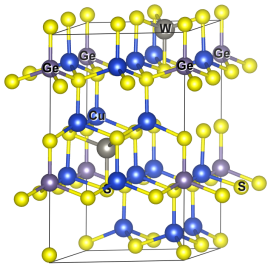

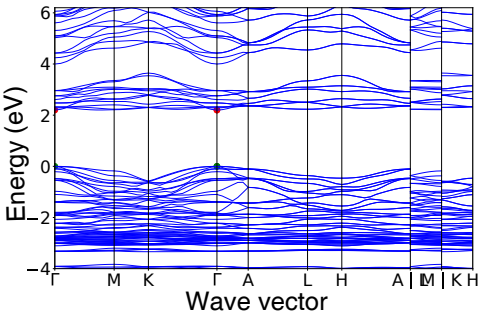

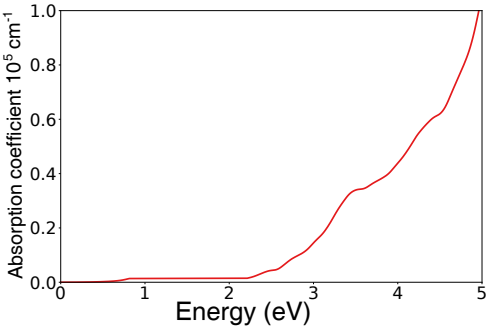

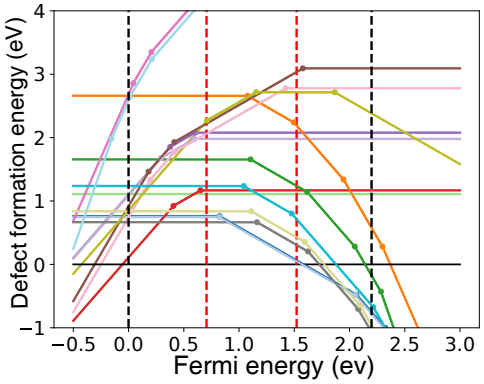

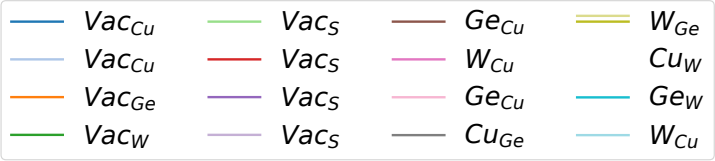

composition	**Cu_8GeS_6**
MP-id	**5546**
space group	**$Pnm2_1$**
hole effective mass	**[1.595, 2.004, 3.245]**
electron effective mass	**[0.179, 0.203, 0.204]**
HSE band gap (indirect/direct) (eV)	**1.9/1.9**
energy above hull (eV/atom)	**0.044**
life time (ns)	**0.0**

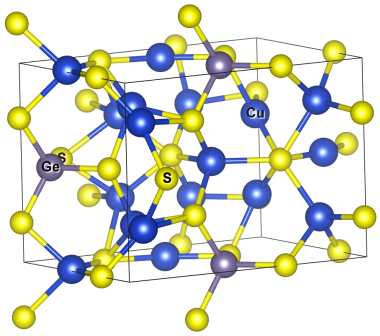

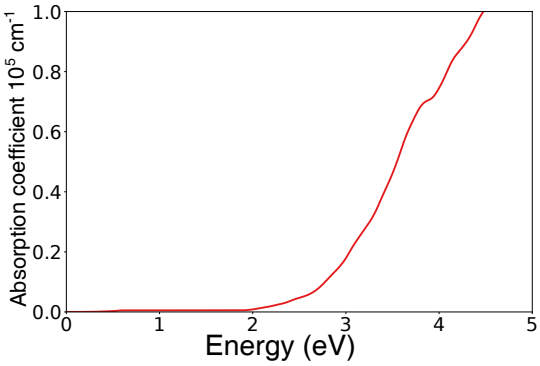

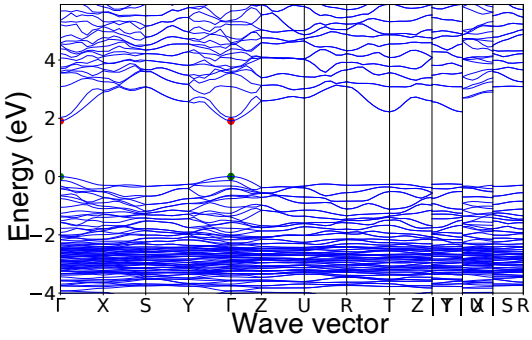

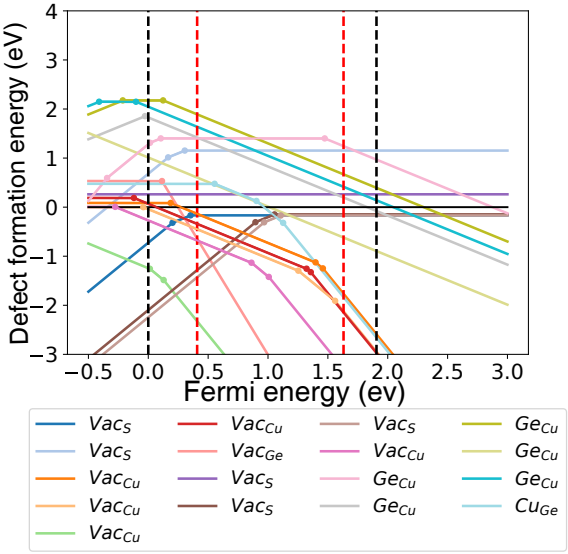

composition	**$SiCu_8Se_6$**
MP-id	**10428**
space group	**Pmn2_1**
hole effective mass	**[1.386, 1.858, 2.572]**
electron effective mass	**[0.126, 0.13, 0.162]**
HSE band gap (indirect/direct) (eV)	**1.47/1.47**
energy above hull (eV/atom)	**0.05**
life time (ns)	**--**

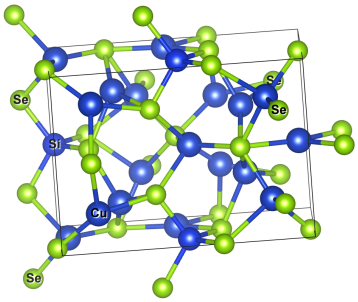

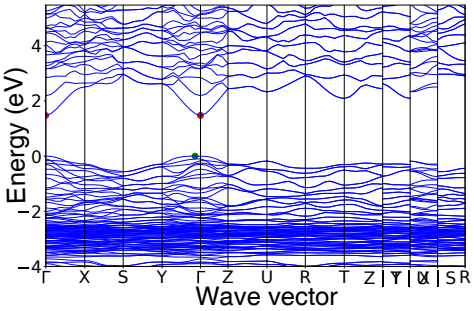

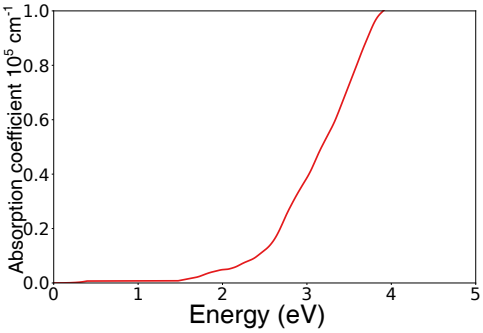

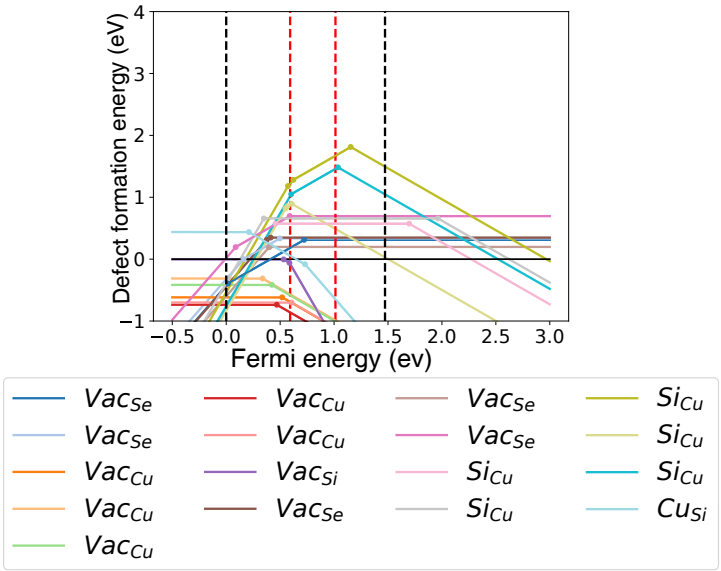

composition	$ErCuSe_2$
MP-id	675180
space group	P3m1
hole effective mass	[0.586, 0.586, 0.927]
electron effective mass	[0.193, 0.193, 0.728]
HSE band gap (indirect/direct) (eV)	2.116/2.2
energy above hull (eV/atom)	0.02
life time (ns)	1.66×10^{-1}

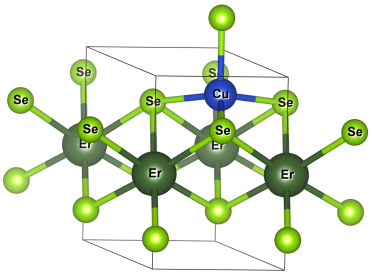

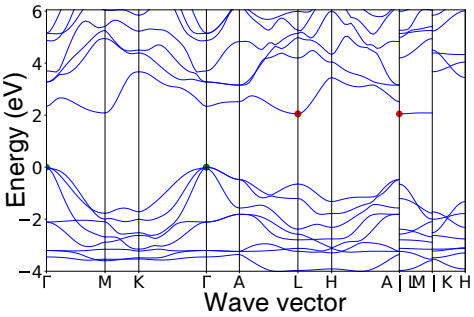

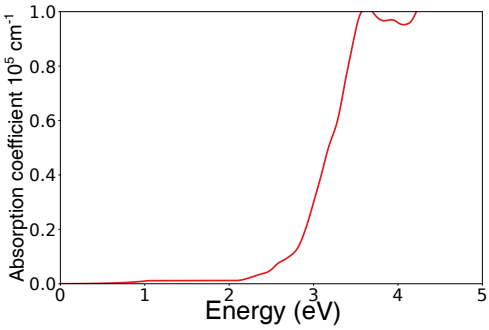

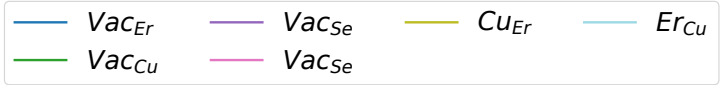

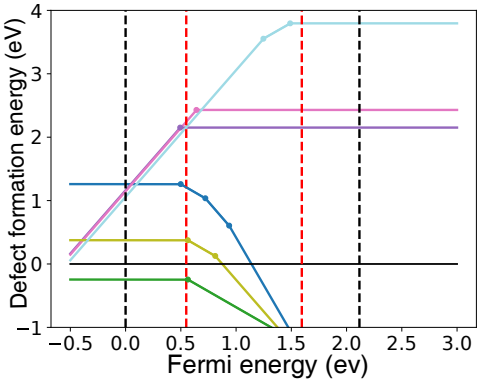

composition	**K_2CuP**
MP-id	**8446**
space group	**P6_3/mmc**
hole effective mass	**[2.175, 2.744, 3.624]**
electron effective mass	**[0.227, 0.754, 0.812]**
HSE band gap (indirect/direct) (eV)	**1.99/1.99**
energy above hull (eV/atom)	**0.0**
life time (ns)	**[3.03−8.5 × 10^{+2}]**

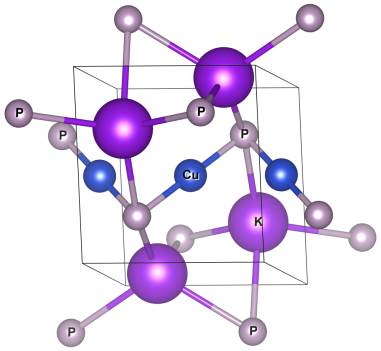

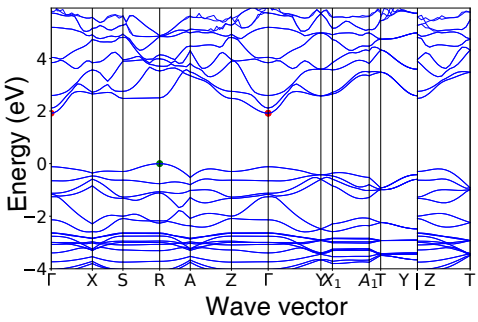

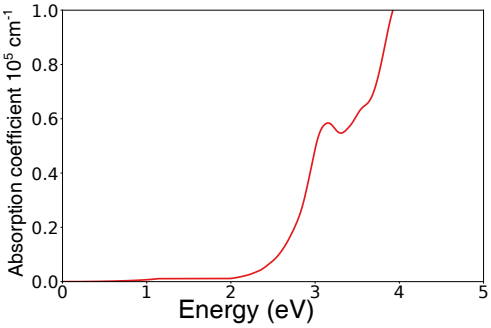

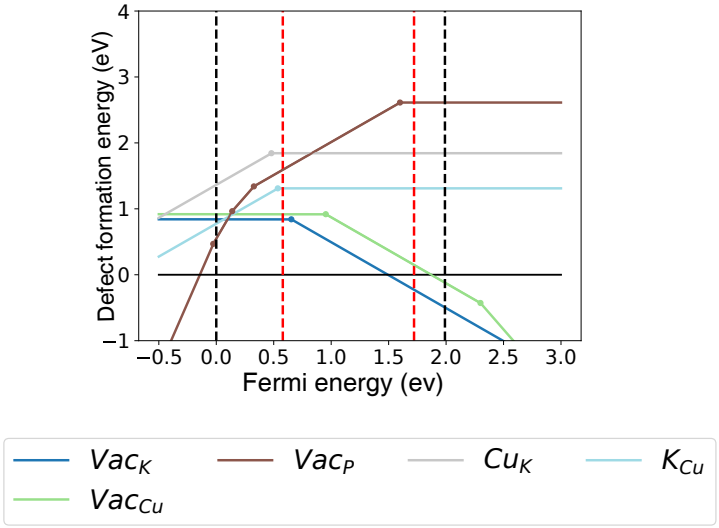

composition	**$K_3Cu_3As_2$**
MP-id	**14205**
space group	**$R\bar{3}m$**
hole effective mass	**[1.272, 1.272, 1.922]**
electron effective mass	**[0.36, 0.36, 0.761]**
HSE band gap (indirect/direct) (eV)	**2.047 / 2.047**
energy above hull (eV/atom)	**0.0**
life time (ns)	**$[3.5\times 10^{-1} - 1.58]$**

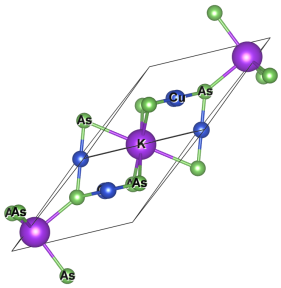

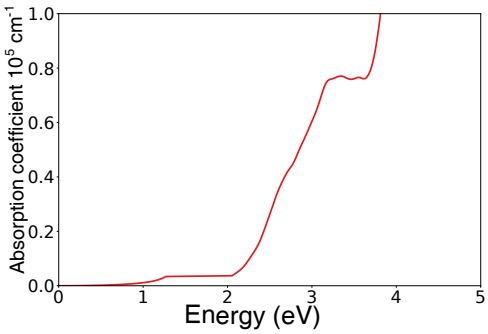

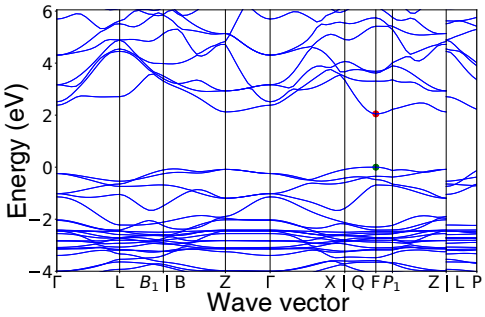

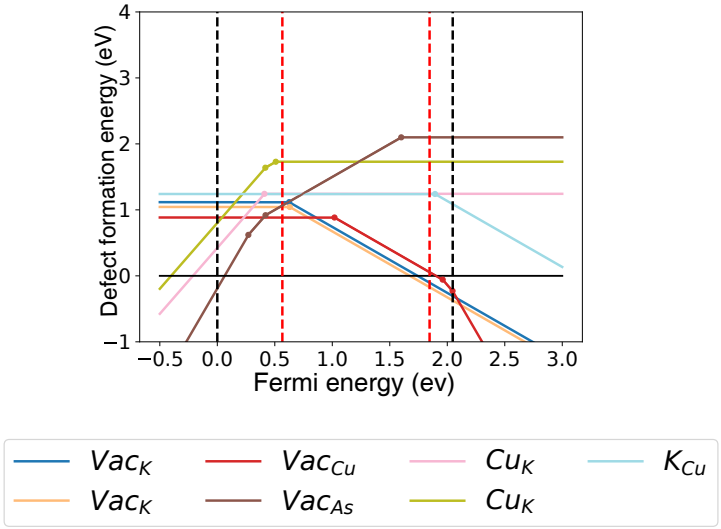

composition	**$K_3Cu_3P_2$**
MP-id	**7439**
space group	**$R\bar{3}m$**
hole effective mass	**[1.236, 1.236, 2.144]**
electron effective mass	**[0.392, 0.392, 0.705]**
HSE band gap (indirect/direct) (eV)	**2.101/ 2.142**
energy above hull (eV/atom)	**0.00**
life time (ns)	**$[3.29-6.7\times10^{1}]$**

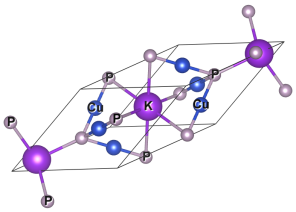

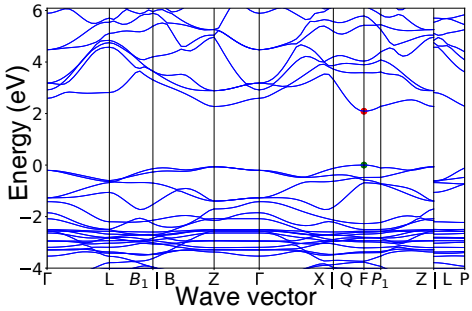

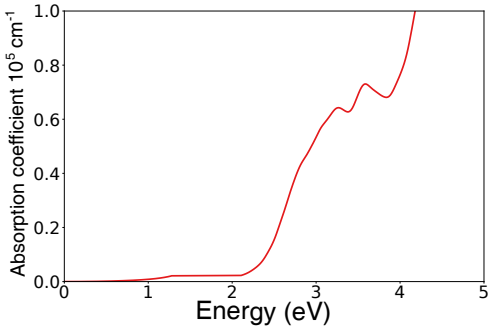

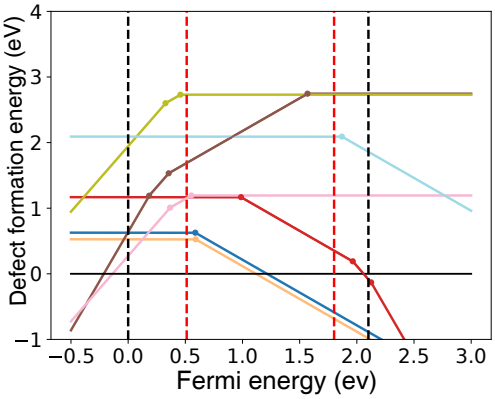

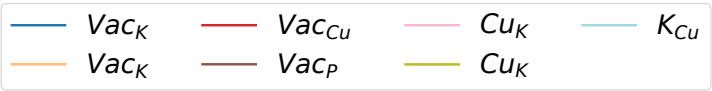

composition	**K_5CuSb_2**
MP-id	**27999**
space group	**$R\bar{3}m$**
hole effective mass	**[2.319, 3.378, 3.378]**
electron effective mass	**[0.19, 0.219, 0.219]**
HSE band gap (indirect/direct) (eV)	**1.44 / 1.59**
energy above hull (eV/atom)	**0.0**
life time (ns)	**2.6**

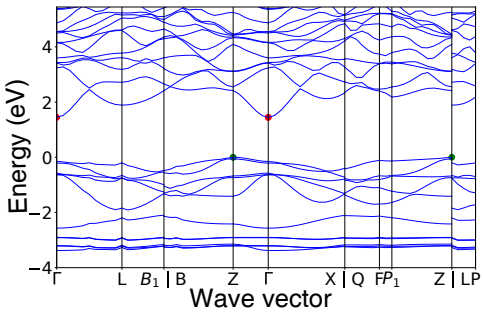

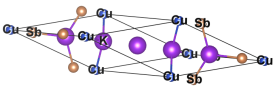

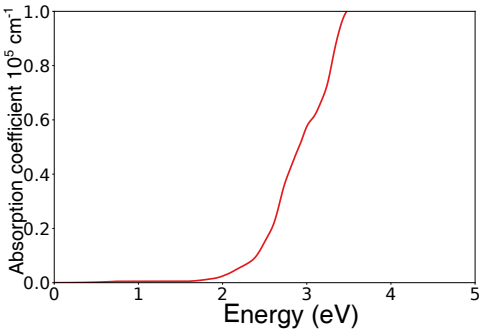

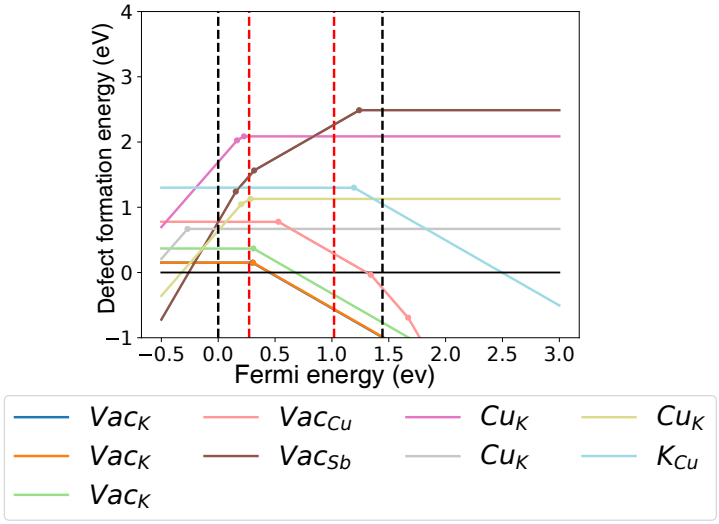

composition	**KCuTe**
MP-id	**7436**
space group	**$P6_3/mmc$**
hole effective mass	**[0.338, 0.338, 6.601]**
electron effective mass	**[0.093, 0.093, 0.432]**
HSE band gap (indirect/direct) (eV)	**1.505/1.505**
energy above hull (eV/atom)	**0.00**
life time (ns)	**>>1**

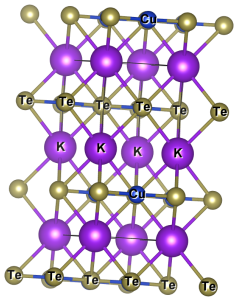

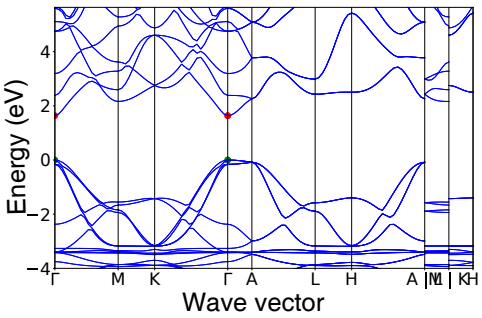

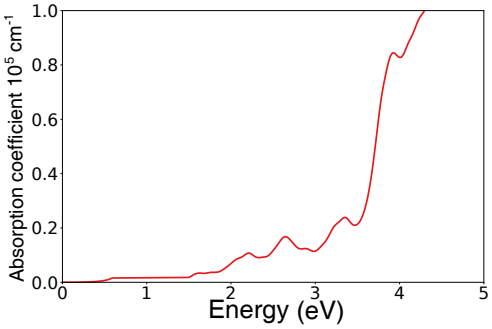

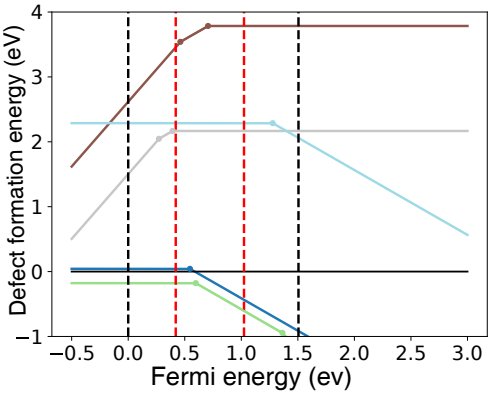

composition	$Li_2Cu_4S_3$
MP-id	766447
space group	Pnma
hole effective mass	[0.263, 0.975, 2.617]
electron effective mass	[0.187, 0.283, 0.438]
HSE band gap (indirect/direct) (eV)	1.94/1.94
energy above hull (eV/atom)	0.077
life time (ns)	--

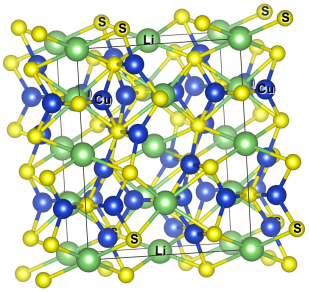

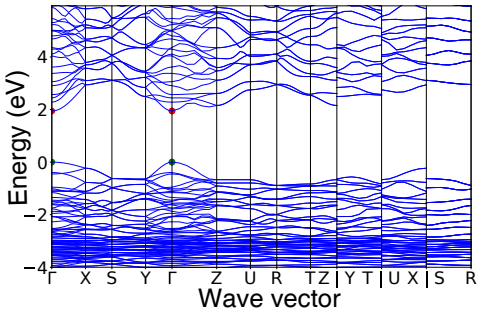

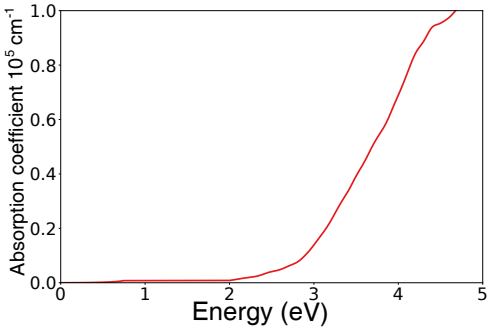

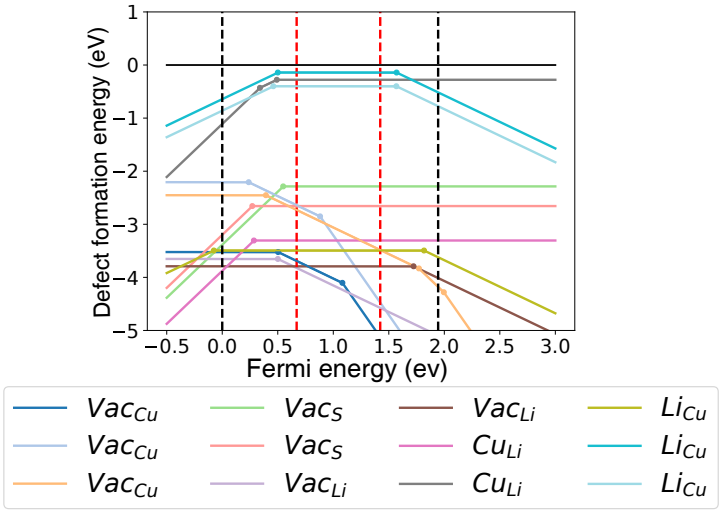

composition	LiCuS
MP-id	753826
space group	Pnma
hole effective mass	[0.419- 1.208- 1.312]
electron effective mass	[0.246- 0.246- 0.298]
HSE band gap (indirect/direct) (eV)	2.297 / 2.297
energy above hull (eV/atom)	0.022
life time (ns)	>>1

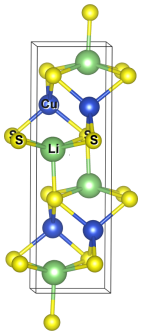

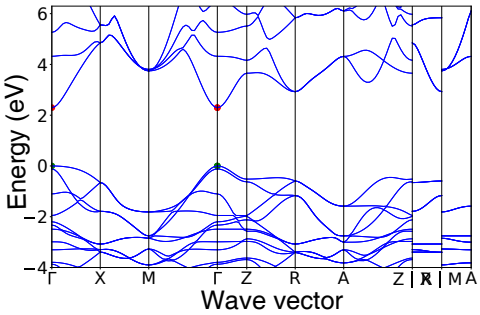

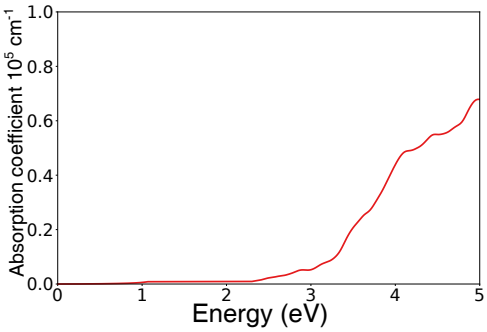

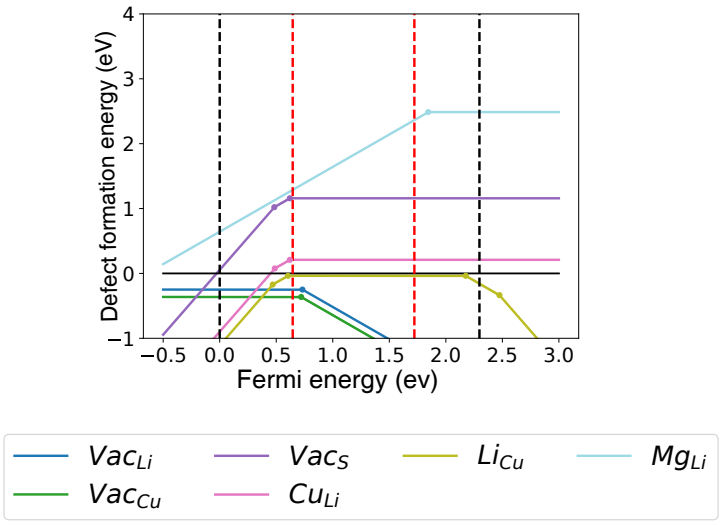

composition	**Na_2CuAs**
MP-id	**15685**
space group	**Cmcm**
hole effective mass	**[0.57, 0.585, 1.438]**
electron effective mass	**[0.159, 0.716, 0.793]**
HSE band gap (indirect/direct) (eV)	**1.289 / 1.365**
energy above hull (eV/atom)	**0.0**
life time (ns)	**>>1**

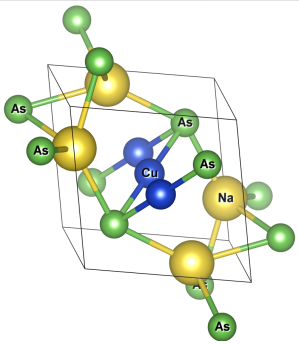

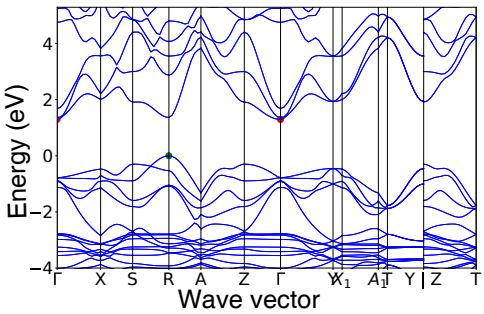

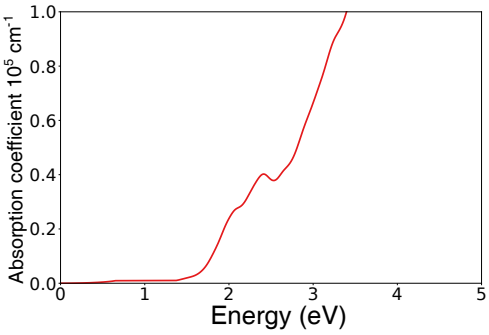

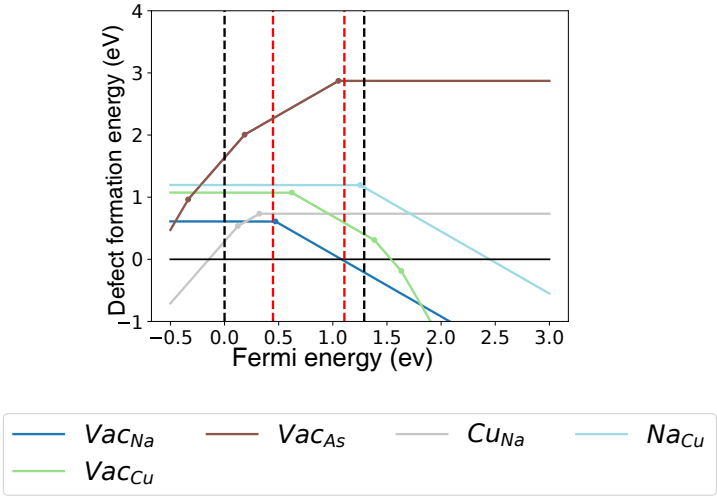

composition	**Na_2CuP**
MP-id	**7639**
space group	**Cmcm**
hole effective mass	**[0.619, 0.731, 1.545]**
electron effective mass	**[0.1, 0.852, 0.898]**
HSE band gap (indirect/direct) (eV)	**1.312 /1.492**
energy above hull (eV/atom)	**0.0**
life time (ns)	**>>1**

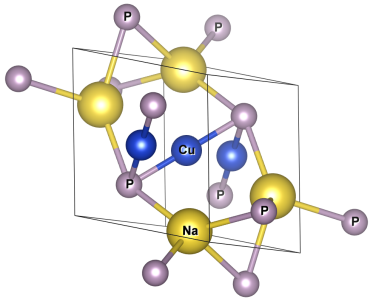

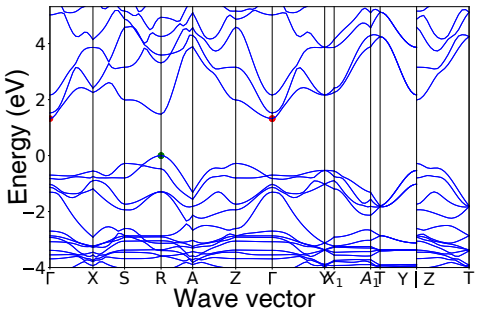

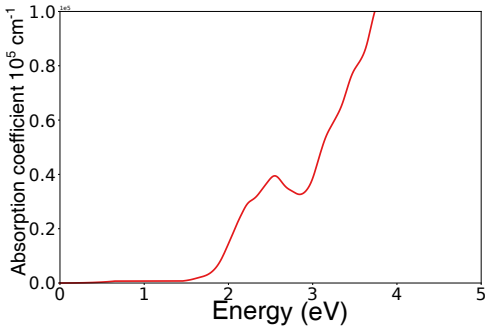

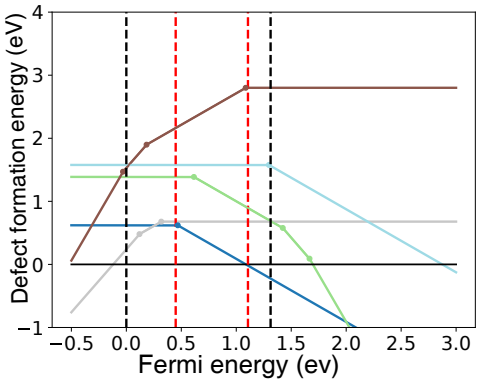

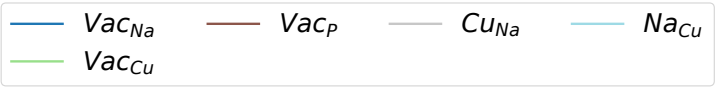

composition	**NaCuTe**
MP-id	**7434**
space group	**P4/nmm**
hole effective mass	**[0.425, 0.425, 1.526]**
electron effective mass	**[0.113, 0.113, 0.133]**
HSE band gap (indirect/direct) (eV)	**1.56 / 1.56**
energy above hull (eV/atom)	**0.01**
life time (ns)	**>>1**

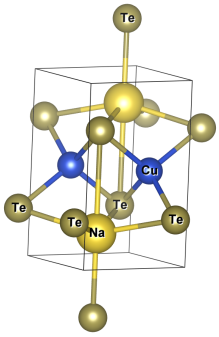

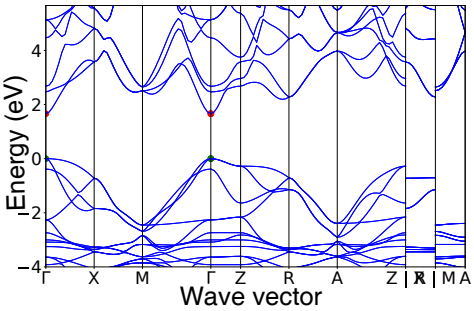

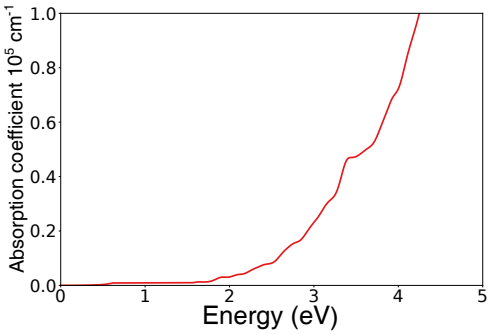

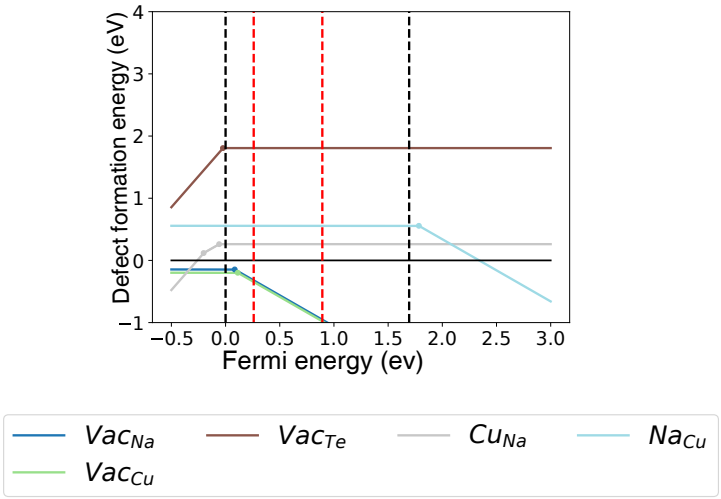

composition	**$Sr_6Cu_3N_5$**
MP-id	**29136**
space group	**$P4_2mc$**
hole effective mass	**[1.525, 5.859, 5.859]**
electron effective mass	**[0.422, 0.607, 0.607]**
HSE band gap (indirect/direct) (eV)	**1.52/1.65**
energy above hull (eV/atom)	**0.00**
life time (ns)	**>>1**

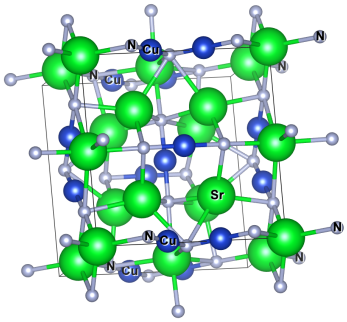

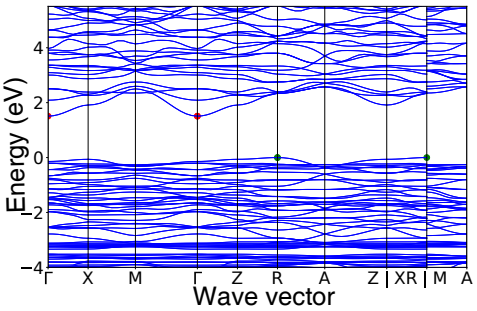

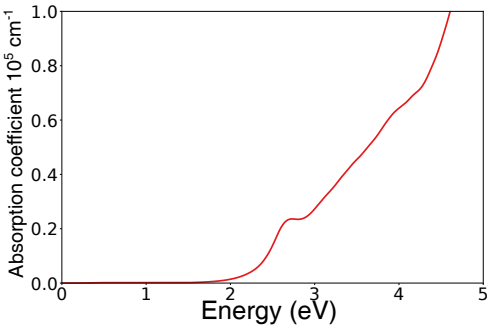

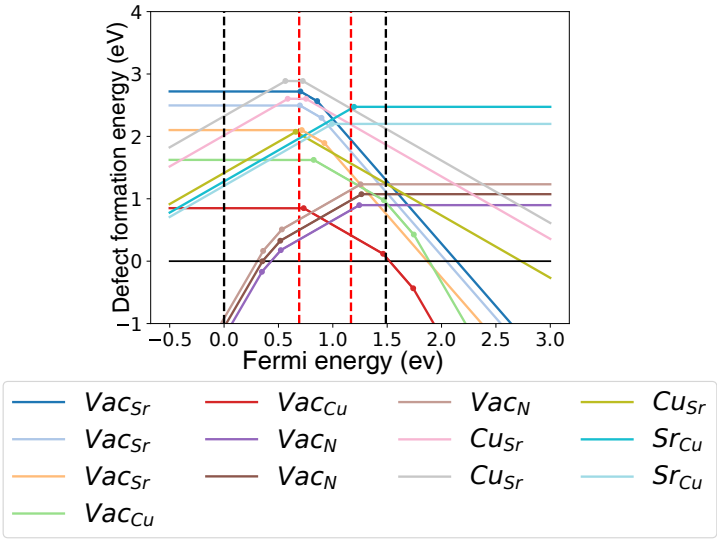

composition	$Y_3CuGeSe_7$
MP-id	17916
space group	$P6_3$
hole effective mass	[0.659, 0.659, 3.915]
electron effective mass	[0.28, 0.645, 0.645]
HSE band gap (indirect/direct) (eV)	2.11/2.117
energy above hull (eV/atom)	0.00
life time (ns)	$[7.01\times 10^{-4} - 7.04\times 10^{-2}]$

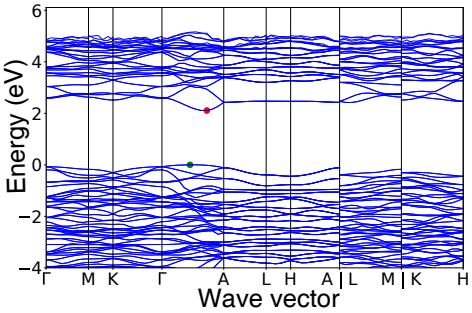

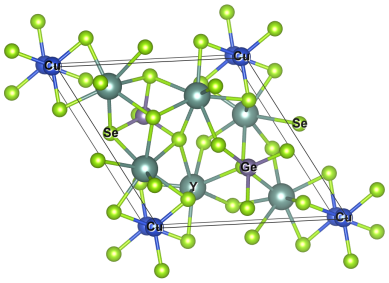

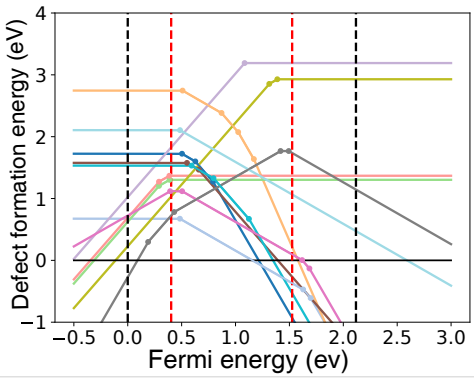

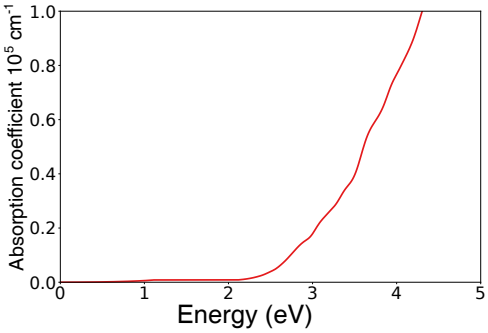

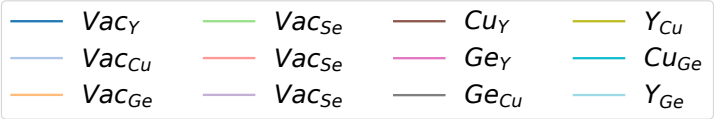

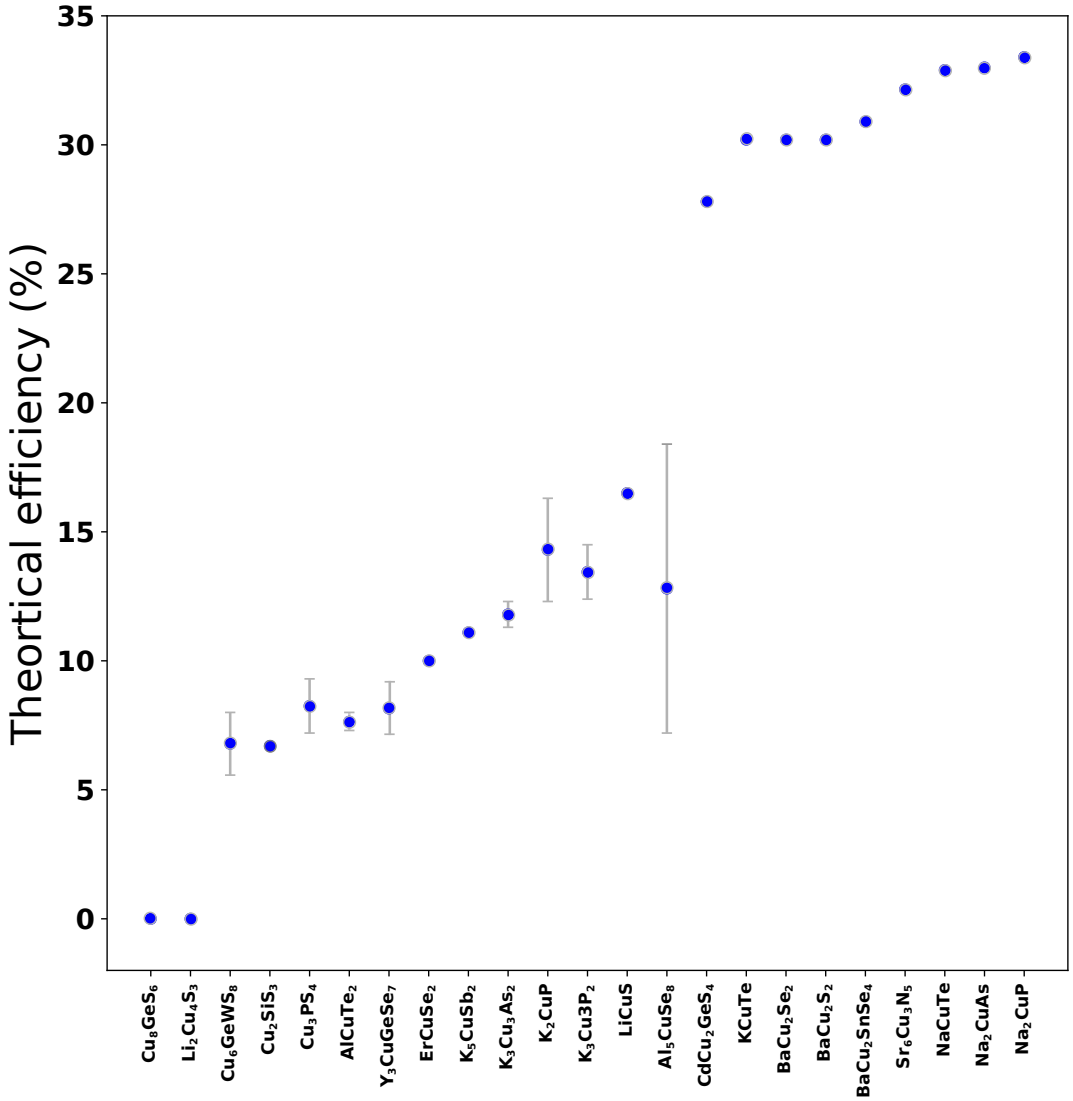

Figure 5: Theoretical efficiency from GGA+HSE approach for the 20 Cu based materials. The range in theoretical efficiency corresponds to different growing conditions, hence different defects present in each material. The middle of the range is indicated by diamonds.

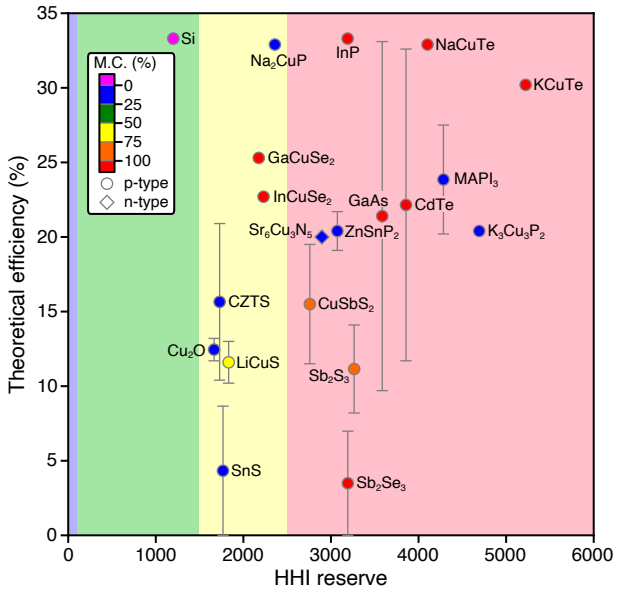

Figure 6: Theoretical efficiency of typical PV absorbers and our outlined candidates versus their reserved HHI. The different colored regions correspond to typical limits. The color of the circles indicates the metal companionality (M.C.) in %.

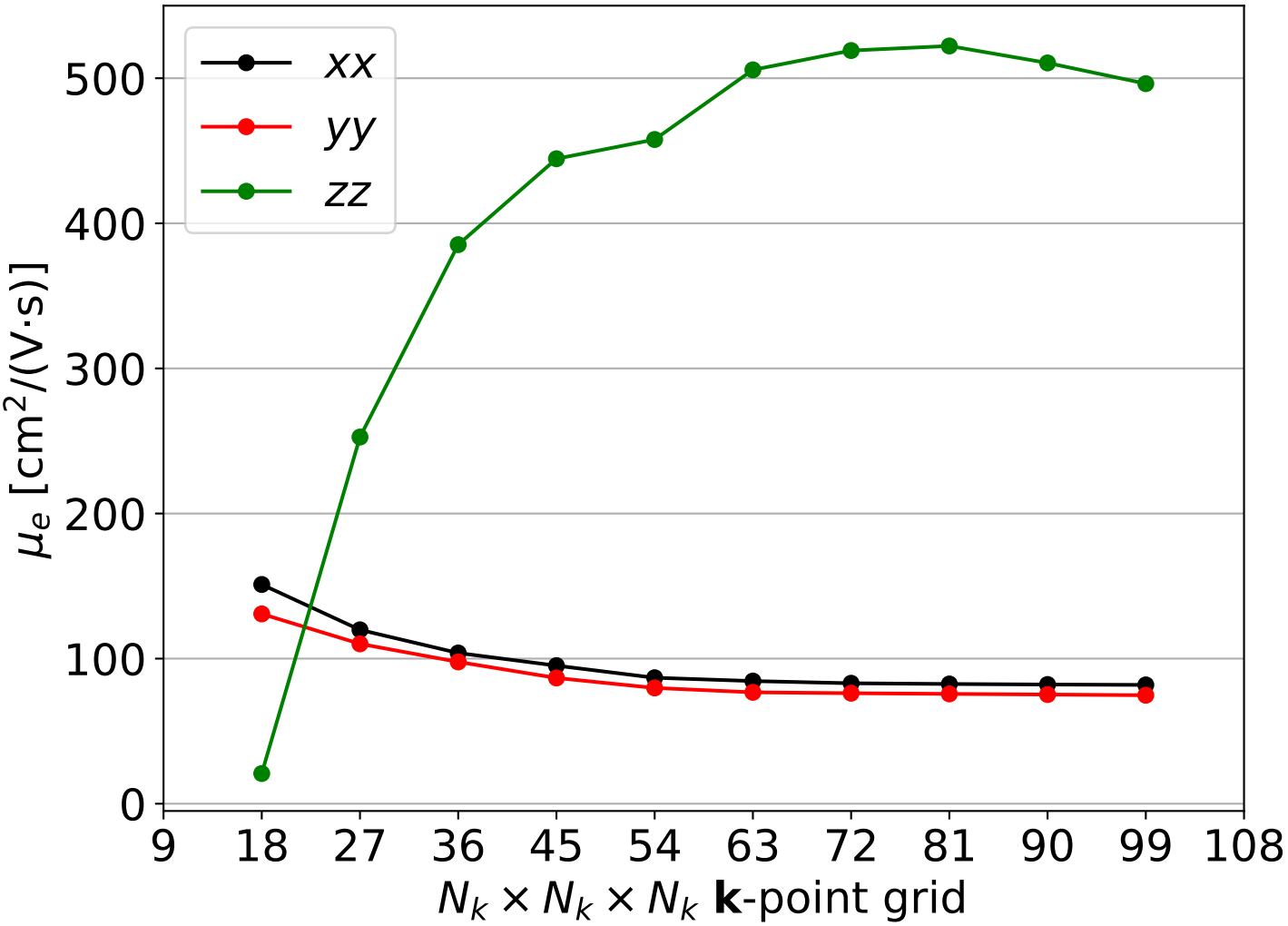

Figure 7: Electron mobility at 300 K in Na_2CuP as a function of the **k** and **q** meshes used for the integrations, see the main text. The **q** is the same as the **k** mesh for the matrix elements but a **q** mesh twice as dense in each direction is used for the energies in the delta distributions for the lifetimes (double-grid method of Ref.[33] The MRTA is used.

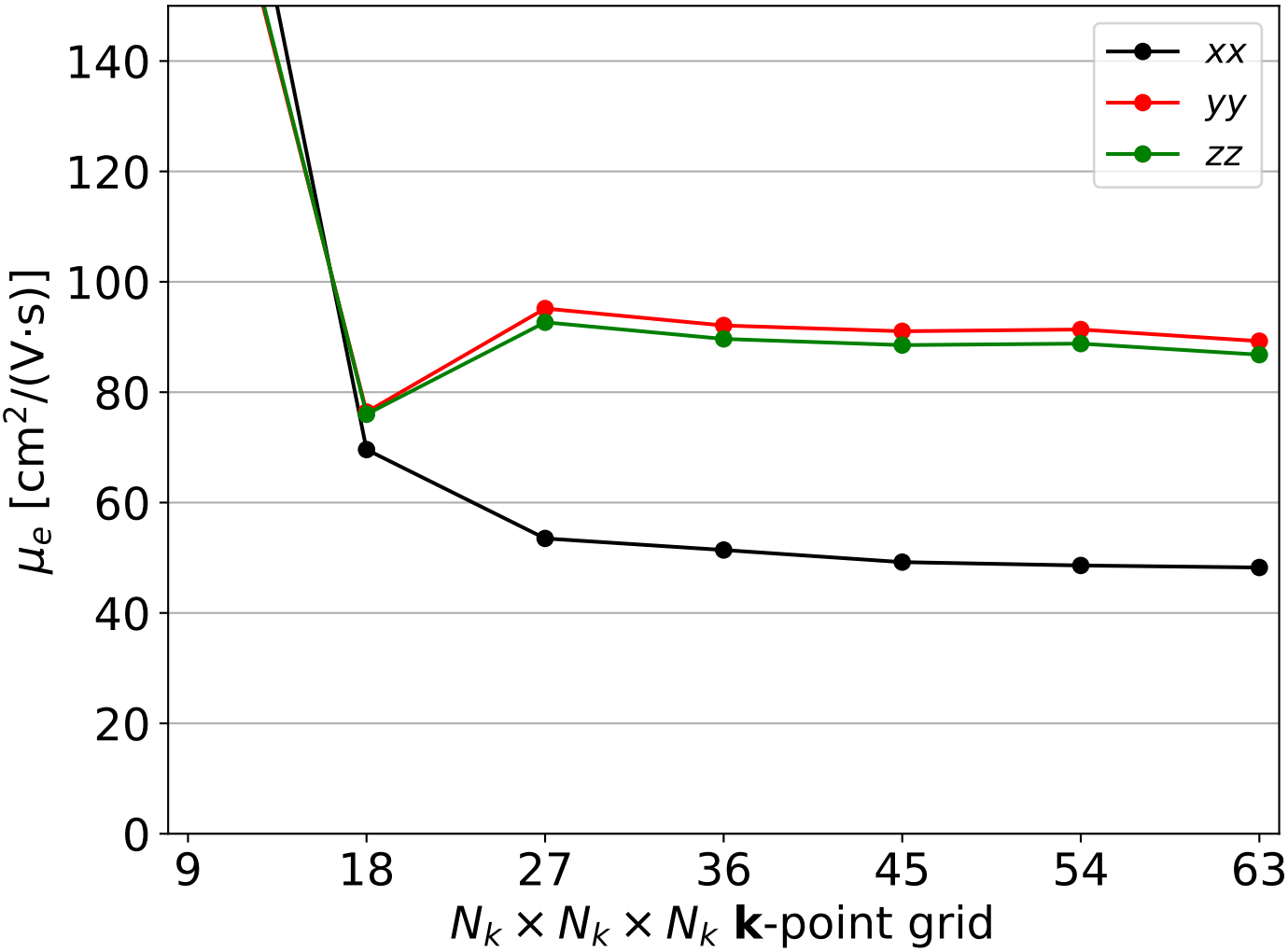

Figure 8: Electron mobility at 300 K in $K_3Cu_3P_2$ as a function of the **k** and **q** meshes used for the integrations, see the main text. The **q** is the same as the **k** mesh for the matrix elements but a **q** mesh twice as dense in each direction is used for the energies in the delta distributions for the lifetimes (double-grid method of Ref.[33] The MRTA is used.

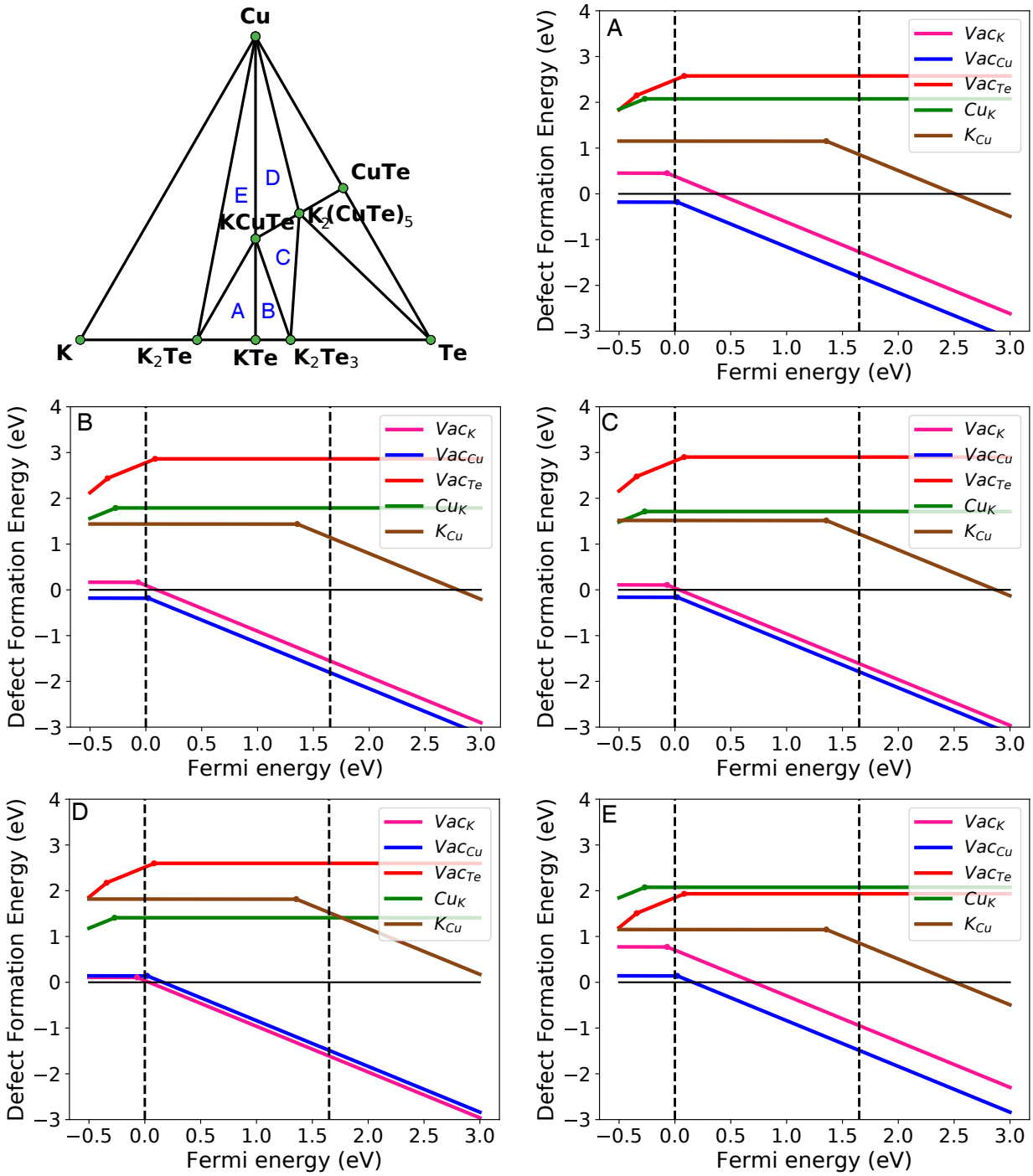

Figure 9: The defect formation energy as a function of Fermi level of intrinsic defects for KCuTe at all possible chemical potentials regions that determined from the facets of the phase diagram.

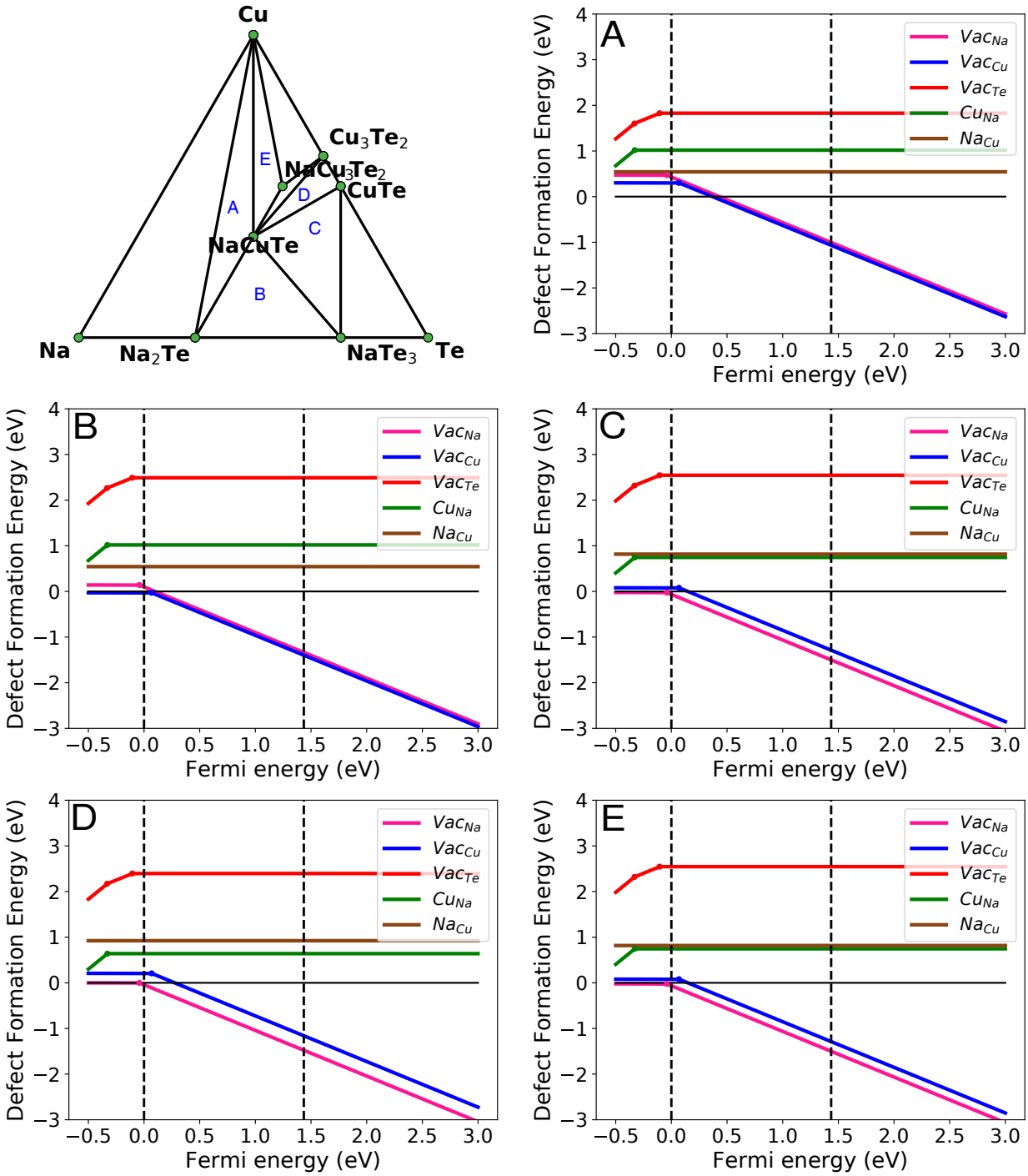

Figure 10: The defect formation energy as a function of Fermi level of intrinsic defects for NaCuTe at all possible chemical potentials regions that determined from the facets of the phase diagram.

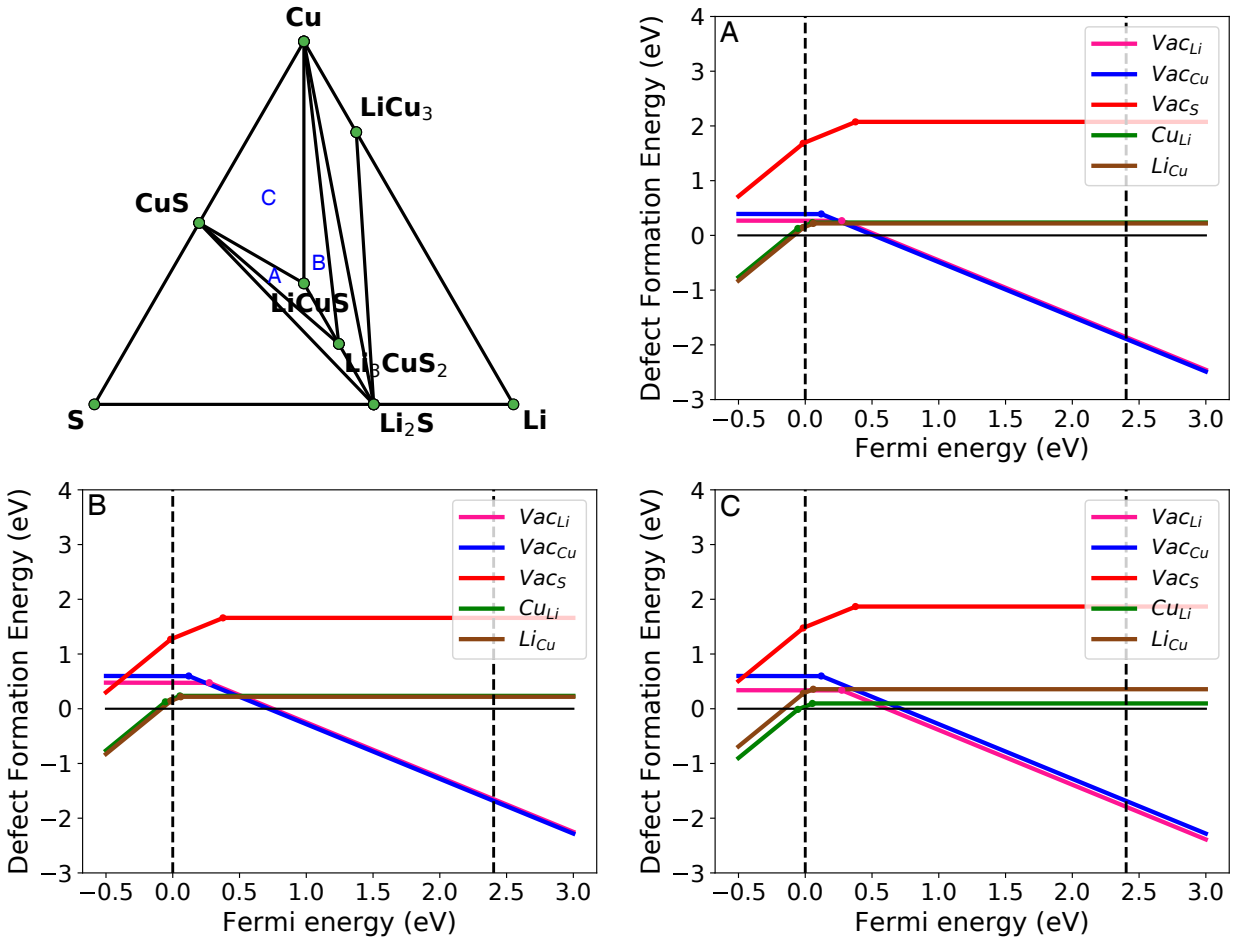

Figure 11: The defect formation energy as a function of Fermi level of intrinsic defects for LiCuS at all possible chemical potentials regions that determined from the facets of the phase diagram.

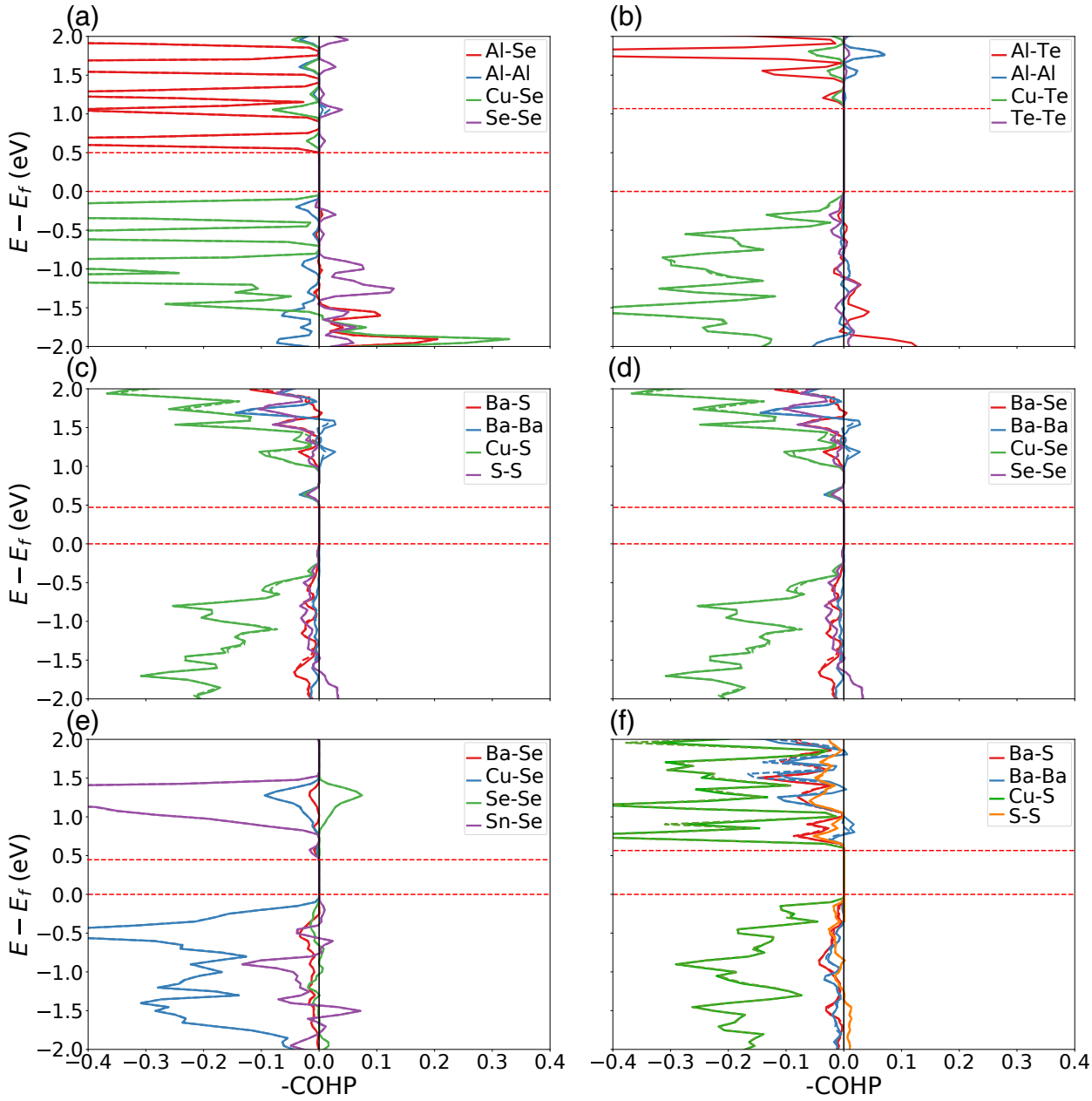

Figure 12: COHP analysis (a,b,c,d,e,f) for all orbitals in pure bulk, averaged for each bond type for Al_5CuSe_8, AlCuTe, $BaCu_2S_2$, $BaCu_2Se_2$, $BaCu_2SnSe_4$, $BaCu_4S_3$.The VBM and CBM are represented by horizontal red dashed lines.

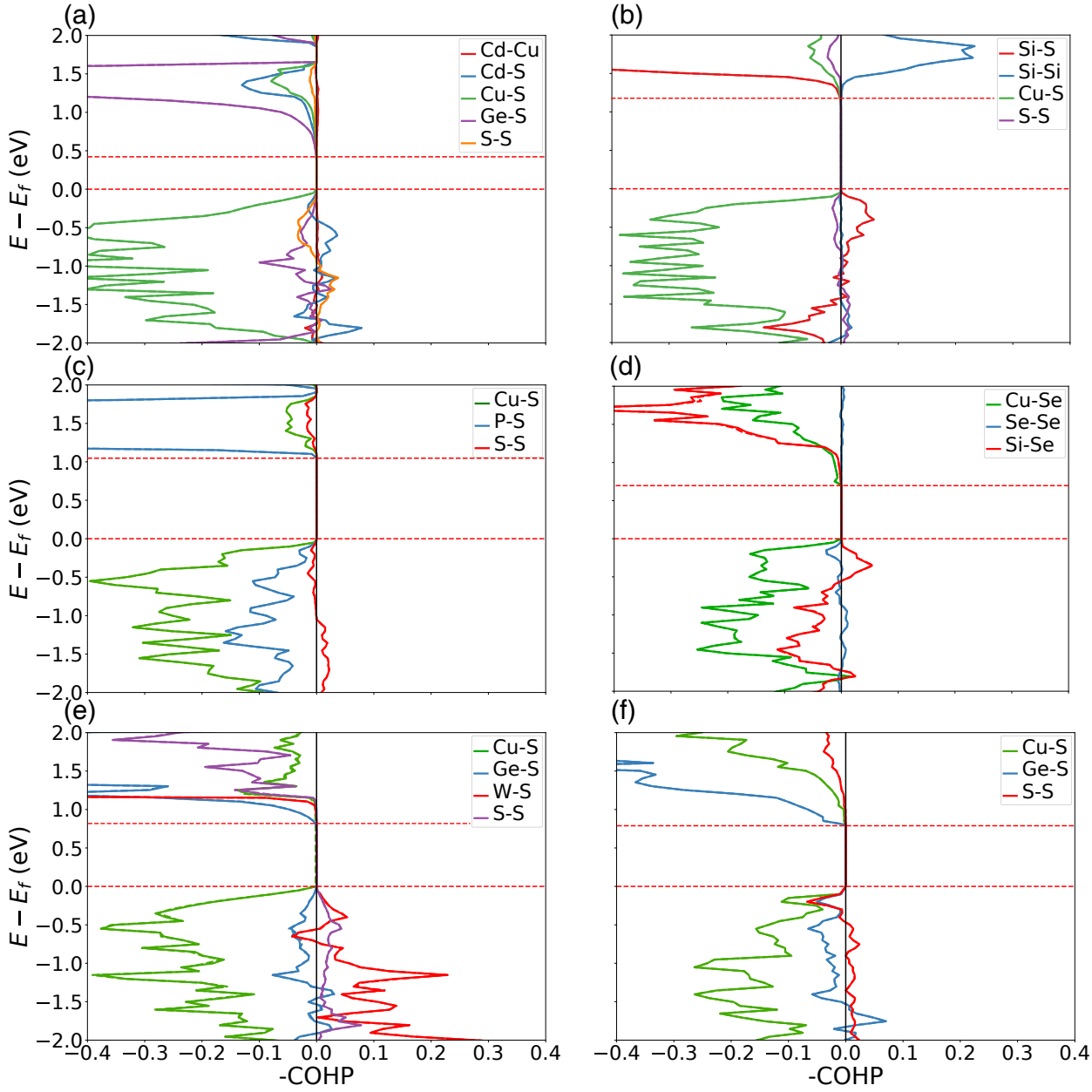

Figure 13: COHP analysis (a,b,c,d,e,f) for all orbitals in pure bulk, averaged for each bond type for $CdCuGeS_4$, Cu_2SiS_3, Cu_3PS_4, Cu_8SiSe_6, Cu_6GeWS_8, Cu_8GeS_6. The VBM and CBM are represented by horizontal red dashed lines.

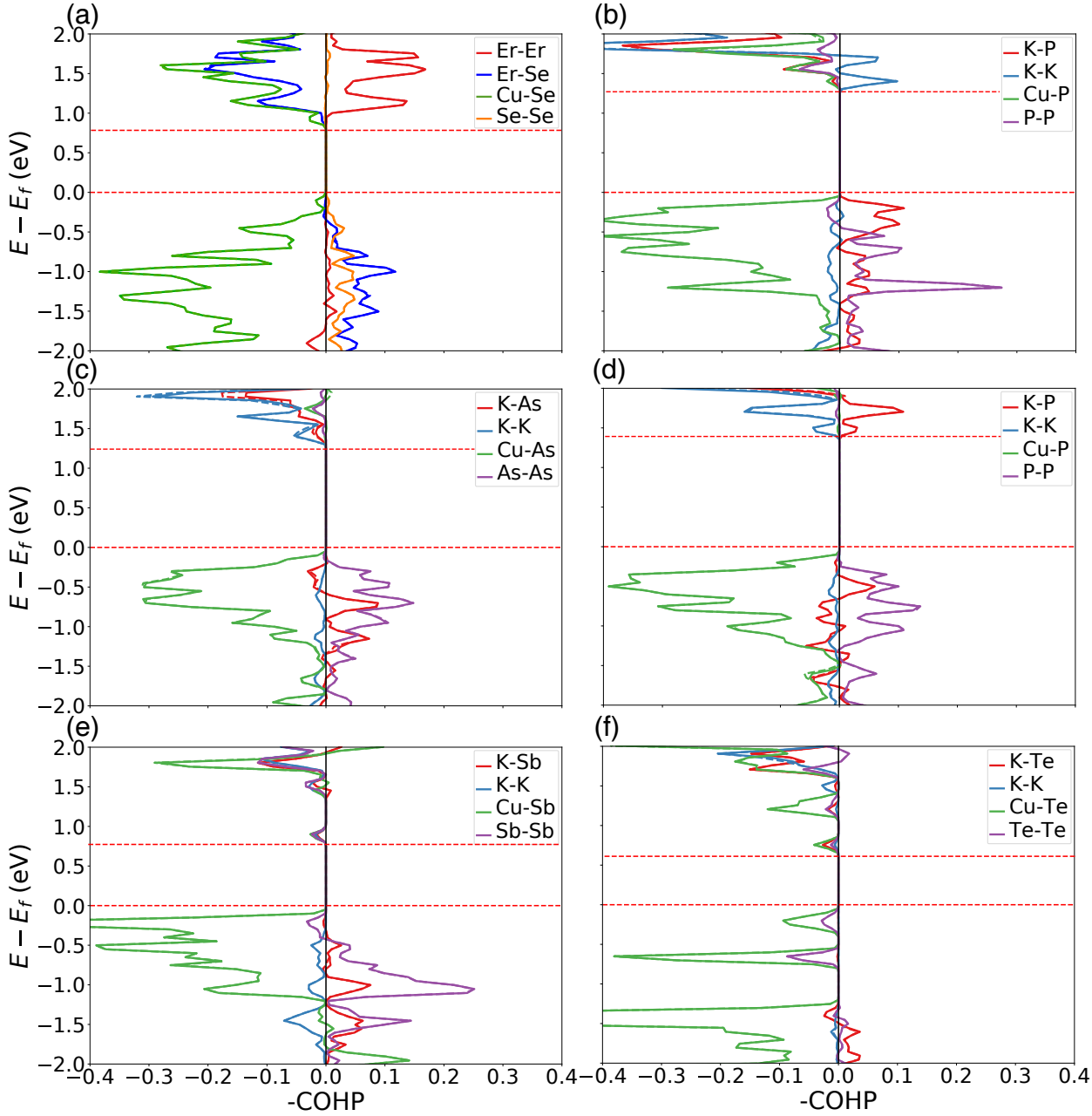

Figure 14: COHP analysis (a,b,c,d,e,f) for all orbitals in pure bulk, averaged for each bond type for $ErCuSe_2$, K_2CuP, $K_3Cu_3As_2$, $K_3Cu_3P_2$, K_5CuSb_2, KCuTe. The VBM and CBM are represented by horizontal red dashed lines

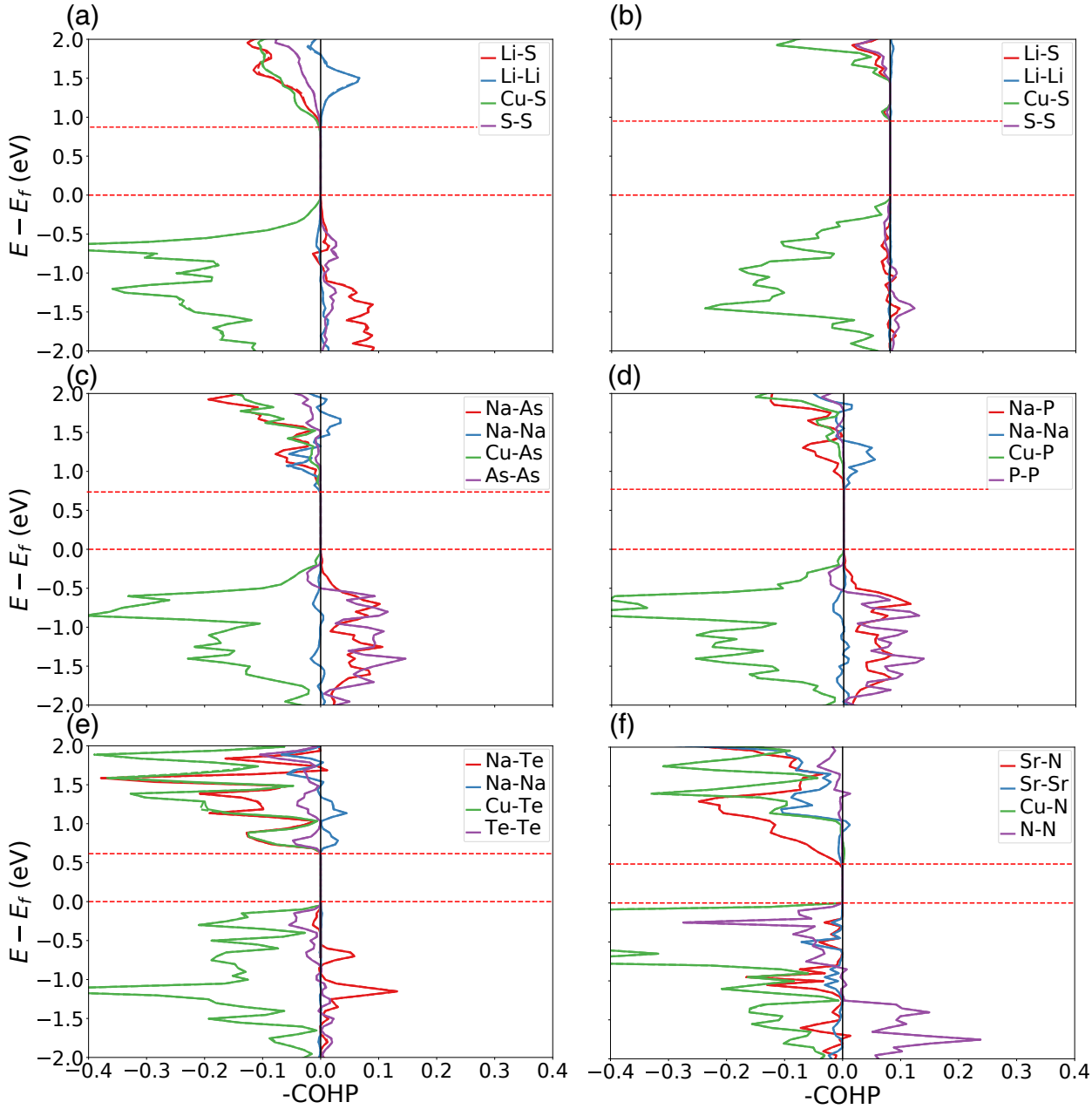

Figure 15: COHP analysis (a,b,c,d,e,f) for all orbitals in pure bulk, averaged for each bond type for $Li_2Cu_4S_3$, LiCuS, Na_2CuAs, Na_2CuP, NaCuTe, $Sr_6Cu_3N_5$. The VBM and CBM are represented by horizontal red dashed lines

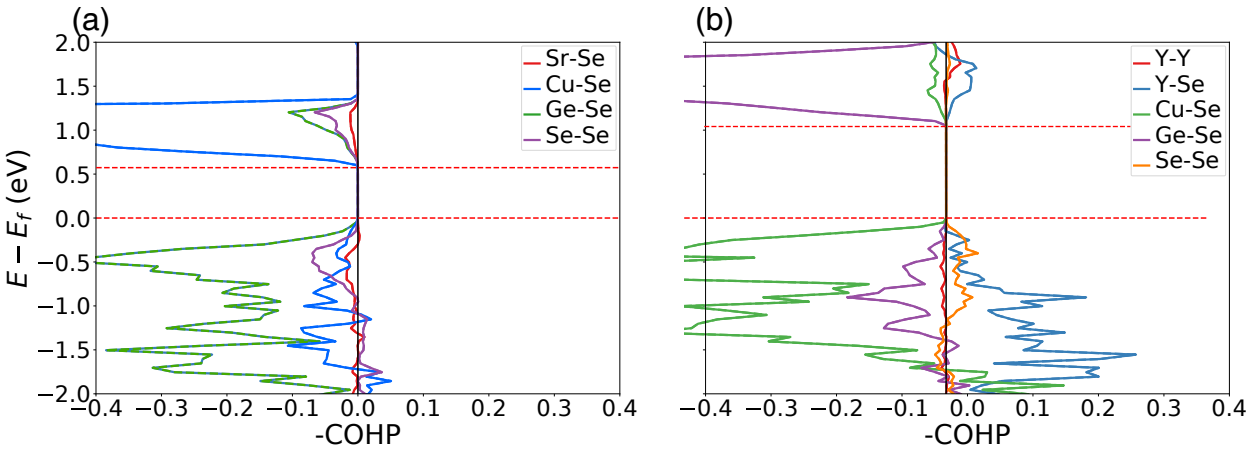

Figure 16: COHP analysis (a,b) for all orbitals in pure bulk, averaged for each bond type for $SrCu_2GeSe_4$, $Y_3CuGeSe_7$. The VBM and CBM are represented by horizontal red dashed lines